



저작자표시-비영리-변경금지 2.0 대한민국

이용자는 아래의 조건을 따르는 경우에 한하여 자유롭게

- 이 저작물을 복제, 배포, 전송, 전시, 공연 및 방송할 수 있습니다.

다음과 같은 조건을 따라야 합니다:



저작자표시. 귀하는 원저작자를 표시하여야 합니다.



비영리. 귀하는 이 저작물을 영리 목적으로 이용할 수 없습니다.



변경금지. 귀하는 이 저작물을 개작, 변형 또는 가공할 수 없습니다.

- 귀하는, 이 저작물의 재이용이나 배포의 경우, 이 저작물에 적용된 이용허락조건을 명확하게 나타내어야 합니다.
- 저작권자로부터 별도의 허가를 받으면 이러한 조건들은 적용되지 않습니다.

저작권법에 따른 이용자의 권리는 위의 내용에 의하여 영향을 받지 않습니다.

이것은 [이용허락규약\(Legal Code\)](#)을 이해하기 쉽게 요약한 것입니다.

[Disclaimer](#)

공학박사 학위 논문

METHODOLOGIES OF MINIMALLY-INVASIVE
DIAGNOSIS AND DRUG THERAPY FOR DIABETES MELLITUS

당뇨병의 최소침습 진단 및 약물
치료를 위한 방법론

2021년 2월

서울대학교 대학원

협동과정 바이오엔지니어링 전공

조 용 찬

METHODOLOGIES OF MINIMALLY-INVASIVE

DIAGNOSIS AND DRUG THERAPY FOR DIABETES MELLITUS

당뇨병의 최소침습 진단 및 약물치료를 위한 방법론

지도 교수 최 영 빈

이 논문을 공학박사 학위논문으로 제출함

2021년 2월

서울대학교 대학원

협동과정 바이오엔지니어링 전공

조 용 찬

조용찬의 공학박사 학위 논문을 인준함

2021년 2월

위원장 김성완

부위원장 최영빈

위원 이정찬

위원 조영민

위원 이동윤



Ph. D. Dissertation

METHODOLOGIES OF MINIMALLY-INVASIVE
DIAGNOSIS AND DRUG THERAPY FOR
DIABETES MELLITUS

BY

YONG CHAN CHO

FEBRUARY 2021

INTERDISCIPLINARY PROGRAM IN BIOENGINEERING

THE GRADUATE SCHOOL

SEOUL NATIONAL UNIVERSITY

METHODOLOGIES OF MINIMALLY-INVASIVE DIAGNOSIS
AND DRUG THERAPY FOR DIABETES MELLITUS

BY

YONG CHAN CHO

FEBRUARY 2021

INTERDISCIPLINARY PROGRAM IN BIOENGINEERING

THE GRADUATE SCHOOL

SEOUL NATIONAL UNIVERSITY

THIS DISSERTATION IS APPROVED FOR
THE DEGREE OF DOCTOR OF PHILOSOPHY

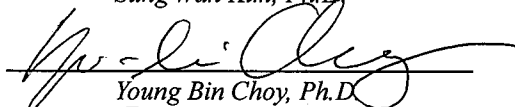
FEBRUARY 2021

DOCTORAL COMMITTEE:

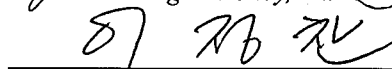
Chairman


Sung Wan Kim, Ph.D.

Vice Chairman


Young Bin Choy, Ph.D.

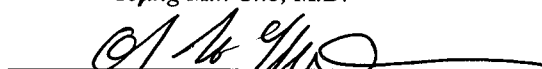
Member


Jung Chan Lee, Ph.D.

Member


Young Min Cho, M.D.

Member


Dong Yun Lee, Ph.D.

Abstract

METHODOLOGIES OF MINIMALLY-INVASIVE DIAGNOSIS AND DRUG THERAPY FOR DIABETES MELLITUS

BY

YONG CHAN CHO

INTERDISCIPLINARY PROGRAM IN BIOENGINEERING

THE GRADUATE SCHOOL

SEOUL NATIONAL UNIVERSITY

This dissertation is focused on design, fabrication and evaluation of a strip-type tear glucose sensor and an implantable magnetic pump for minimally-invasive diagnosis and drug therapy, respectively.

Management of diabetes mellitus have been painful procedures to many patients, because the diagnosis included needled finger pricking with a lancet, and the drug therapy were conducted with needled injections. There have been

research efforts to minimize the pain associated with the diabetes mellitus management, but still there are unmet drawbacks. Therefore, methodologies of minimally-invasive diagnosis and drug therapy are proposed in this study.

First, a strip-type tear glucose sensor was developed for concurrent tear collection and measurement with a small tear volume. Current tear glucose measurement has drawbacks such as large tear sample volume, long tear collection time, discomfort to patients, and two-step procedure that require sample transfer from tear collector to measuring instruments. To resolve these issues, a highly-accurate strip-type electrochemical sensor was modified by reducing the volume of reaction chamber to 0.4 μl . Then the modified sensor and a 3D printed lid to ensure safety to the eye were assembled. The assembled sensor, or the tear-glucose device, could collect tear fluid sample within 2 seconds, and simultaneously measure tear glucose concentration accurately without sample transfer. Through animal experiments, a high correlation between tear glucose concentration and the blood glucose concentration were determined with the tear-glucose device. The Clarke error grid analysis suggested that the blood glucose concentration estimated from the tear glucose sensor showed acceptable accuracy compared to that measured with commercially available blood glucometer.

In addition, an implantable magnetic pump enabled with on-demand bolus delivery of exenatide was developed. The magnetic pump could deliver a bolus of $11.4 \pm 0.3 \mu\text{g}$ of exenatide for optimal exenatide delivery regimen. This magnetic pump was designed to be actuated with a patterned magnetic field, thus could prevent unintended actuations by a single household magnet. In addition, a flexible polyurethane drug container in the magnetic pump could

resolve negative pressure issues that could occur in solid drug container. The magnetic pump could deliver up to 300 times without a drug replenishment. The absence of battery and the presence of refillable drug container enabled a semi-permanent usage of the magnetic pump. The magnetic pump showed a similar pharmacokinetic profile compared to the injection therapy. When implanted in type 2 diabetic animal models, the magnetic pump showed comparable efficacy to injection therapy, in terms of body weight change, food intake, glycemic control, insulin secretion, insulin sensitivity, gastric emptying rate, beta cell proliferation and adipocyte size reduction.

Through these studies, it is concluded that the strip-type tear glucose sensor and the magnetically actuated pump developed herein could be suggested as methodologies to replace invasive finger pricking and injection therapy.

Keywords : Minimally-invasive, Diabetes mellitus, Blood glucose measurement, Tear glucose measurement, Strip-type tear glucose sensor, Needled injection, Magnetically-actuated, Implantable drug delivery device

Student number: 2017-33892

Contents

Abstract	i
Contents	iv
List of Tables	vii
List of Figures	viii
Chapter 1. Introduction	1
1.1. Current management methodologies for diabetes mellitus.....	1
1.2. Tear-based methodologies of minimally-invasive diagnosis for diabetes mellitus	3
1.3. Implantable drug delivery device for minimally-invasive drug therapy for diabetes mellitus.....	5
1.4. Current limitations and research aims	7
Chapter 2. Strip-type tear glucose sensor for concurrent tear collection and glucose measurement	9
2.1. Device design	9
2.2. Methods	11
2.2.1. Lid	11
2.2.2. Strip-type glucose sensor	14

2.2.3. In vitro evaluation	15
2.2.4. In vivo evaluation	17
2.2.5. Statistical analysis	18
2.3. Results	18
2.3.1. Tear-glucose device	18
2.3.2. In vitro performance evaluation	20
2.3.3. In vivo performance evaluation	20
2.3.4. In vivo safety evaluation	26
2.4. Discussions	28

Chapter 3. Implantable magnetic pump for bolus delivery of exenatide 33

3.1. Device design	33
3.2. Methods	35
3.2.1. Materials	35
3.2.2. Magnetic pump fabrication	35
3.2.3. Magnetic design principles	38
3.2.4. High-performance liquid chromatography measurements	38
3.2.5. In vitro performance test	38
3.2.6. Accelerated depletion test	39

3.2.7. Stability evaluation of exenatide	39
3.2.8. Animal study	40
3.2.9. Glucose tolerance test	43
3.2.10. Paracetamol absorption test	43
3.2.11. Histology and immunohistochemistry	43
3.2.12. Statistical analysis	44
3.3. Results	45
3.3.1. Pump design and working principles	45
3.3.2. In vitro performance test	52
3.3.3. In vivo pharmacokinetic tests	57
3.3.4. In vivo pharmacodynamic tests	62
3.3.5. Effects on the pancreatic islets and adipose tissues	70
3.3.6. Biocompatibility assessment	77
3.4. Discussions	82
Chapter 4. Conclusion and perspective	86
References	89
Abstracts in Korean	97
Acknowledgement	100

List of Tables

Table 3.1	Assessment of inflammatory markers in plasma	81
------------------	--	----

List of Figures

Figure 2.1	Schematic images of the lid for minimally-invasive tear collection	12
Figure 2.2	Optical images of the lid for minimally-invasive tear collection	13
Figure 2.3	Modification of strip-type glucose sensors	16
Figure 2.4	Preparation of the tear-glucose device	19
Figure 2.5	Calibration curve for varying glucose concentrations obtained with the tear-glucose device	21
Figure 2.6	Correlation between blood glucose concentrations and tear glucose concentrations obtained with the tear-glucose device from all eight rabbits (i.e., eight eyes) employed in this work	22
Figure 2.7	Correlation between average glucose concentrations in tear and blood obtained at each scheduled time of measurements	23
Figure 2.8	Clarke error grid analysis on blood glucose concentrations obtained with the tear-glucose device and a clinically approved glucometer	25
Figure 2.9	Representative fluorescent images obtained from the IPCs of fluorescein-stained rabbit eye	27

Figure 2.10	Temporal correlation between blood and tear glucose concentrations, which were measured by a glucometer and tear-glucose device herein, respectively	31
Figure 2.11	Device evaluation at the range of glucose concentration in human tear fluids	32
Figure 3.1	Detailed description of the magnetic pump fabrication procedures	37
Figure 3.2	Surgical procedure for the magnetic pump implantation and exenatide replenishment	41
Figure 3.3	Timeline of the study events	42
Figure 3.4	3D schematic of the pump	47
Figure 3.5	Refill port after implantation	48
Figure 3.6	Optical image of the pump and external device with patterned magnets	49
Figure 3.7	Actuation principle of the pump	51
Figure 3.8	In vitro performance test of the magnetic pump	53
Figure 3.9	In vivo pharmacokinetic profiles of exenatide	58
Figure 3.10	Reproducibility assessment of the magnetic pump after a replenishment in vivo	60
Figure 3.11	Pharmacodynamic profiles of exenatide	64
Figure 3.12	Profiles of pancreatic islet structure	71

Figure 3.13	Profiles of adipocytes in the epididymal fat pad in GK rats	73
Figure 3.14	Number of crown-like structures in epididymal adipose tissues	75
Figure 3.15	Representative H&E-stained images of (A) subcutaneous and (B) brown adipose tissues	76
Figure 3.16	Histological images of the tissues around the implanted magnetic pump	78

Chapter 1

Introduction

1.1 Current management methodologies for diabetes mellitus

Diabetes mellitus is a chronic disease characterized by elevated plasma glucose level (1, 2). There are two types of diabetes mellitus that require long-term management. Type 1 diabetes mellitus (T1D) is characterized by insulin deficiency caused by beta-cell destruction in pancreas. Type 2 diabetes mellitus (T2D) is characterized by relatively insufficient insulin secretion due to insulin resistance, affected by genetic and environment factors such as diets or exercises. Both types of diabetes mellitus require frequent diagnosis and adequate drug therapy to prevent progression of symptoms or complications (3, 4). Because diabetes mellitus are ongoing chronic diseases, often these management lasts from years to one's lifetime.

Currently, diabetes mellitus is initially diagnosed through measuring fasting

glucose, random glucose, 2-hour glucose after oral glucose tolerance test, or HbA1C. For daily-life management of diabetes mellitus, usually the blood glucose level is measured by patients themselves for multiple times a day. For this, patients draw a drop of blood through finger pricking with a sterile lancet, and use a glucometer to calculate blood glucose concentration (5).

The drug therapies are different between the two types of diabetes mellitus. As patients with T1D do not produce sufficient amount of insulin, it is essential to inject insulin to lower the glucose level after meal. For T2D, behavioral changes and oral noninsulin medications are recommended first, and then injectable medications are prescribed. Representative oral noninsulin medications include metformin that reduces glucose formation from liver, sulfonylurea that increases insulin production, and thiazolidinedione to reduce insulin resistance (6).

Injectable medications include insulin or glucagon-like peptide-1 (GLP-1) receptor agonists (RA). Insulin lowers blood glucose level by facilitating storage of glucose into muscle cells, liver cells, and adipocytes. However, the insulin injection always accompanies risks of hypoglycemia, and thus require more frequent monitoring of blood glucose. On the other hand, GLP-1 RA is relatively free from hypoglycemia. GLP-1 RA is reported to control blood glucose level but not induce hypoglycemia by increasing insulin secretion with elevated glucose level, decreasing glucagon secretion, and enhancing insulin sensitivity. Furthermore, it reduces gastric emptying rate and appetite to help lowering glucose concentration in plasma.

However, many patients with either type of diabetes mellitus measure plasma glucose level multiple times a day by drawing blood with a lancet, and

administer insulin or noninsulin medications through needed injection or infusion. Both diagnosis and treatment cause discomfort and pain, also may further cause trauma, callus formation, pruritus, or inflammation (7, 8). These side effects associated with glucose measurement and drug administration cause a significant portion of patients to intentionally omit the scheduled diagnosis or drug therapy, hence suboptimal management and increased cost of management (9-11). To resolve this issue, minimally-invasive alternative methodologies are needed.

1.2 Tear-based methodologies of minimally-invasive diagnosis for diabetes mellitus

Recently, many research approaches were made to replace needed diagnosis. For this, bodily fluids other than blood (i.e. saliva, sweat, urea, tear and interstitial fluid) were tested for indirect measurement of plasma glucose (12). Among them, glucose measurement through tear fluid has drawn a great deal of interest. The glucose level in tears is known to have a demonstrable correlation with that in blood (13), and tears can be collected relatively easily from the anterior space of the eye, which can be less invasive compared with conventional blood withdrawal through skin punctures. Many studies utilized powerful analytical tools or glucose oxidation to assess the correlation because the glucose concentration in tear fluid is reported to be 30-50 times lower than the blood glucose concentration (14).

A liquid chromatography and electrospray ionization mass spectrometry (LC/ESI-MS) was used to determine the glucose concentration in tear. A representative study was conducted by Baca et al. (15). They collected 1 μ l of

tear fluids from fasting human subjects with a glass capillary tube under monitoring with a slit lamp microscope, and analyzed the glucose concentration with LC/ESI-MS. They observed that the fasting tear glucose concentrations from nondiabetic subjects is lower than the generally reported normal tear glucose concentration from nondiabetic subjects, thereby suggesting correlation between the tear and the blood glucose level.

A diffuse reflectance polarization imaging system was developed to utilize the spectroscopic properties of glucose molecules to determine the glucose concentration in tear fluid samples. Cameron et al. developed a diffuse reflectance polarization imaging system to assess the rotation of polarized light according to the glucose concentration (16). Stuart et al. used near-infrared surface-enhanced Raman spectroscopy and a gold nanosphere platform (17). They measured the energy absorbed by glucose sample to determine the glucose concentration.

Electrochemical sensors that catalyze glucose oxidation to generate current was developed to measure tear glucose concentrations. There are enzymatic and non-enzymatic electrochemical sensors. Enzymatic electrochemical sensors use glucose oxidase or glucose dehydrogenase, along with electron transfer cofactors (i.e. flavin adenine dinucleotide and pyrroloquinoline quinone, respectively) to facilitate the oxidation reaction of a β -D-glucose molecule to generate a D-glucono-1,5-lactone molecule and reduced electron transfer cofactors. The electron in the electron transfer cofactor is then transferred to electrodes via hydrogen peroxide, electron mediator or direct transfer (18). Non-enzymatic electrochemical sensors are made of various materials, such as platinum or gold (19). The electrodes provide electric potential sufficient to

oxidize glucose molecule on the electrode surface. One of the recent electrochemical tear glucose sensor is introduced by Peng et al (20). They developed a glucose oxidase-based electrochemical sensor in a shape of thin wire, so that the sensor can be inserted into the glass capillary tube after tear collection.

A glucose oxidase-coupled DNAzyme sensor was reported by Liu et al. (21). The sensor is a dual enzyme sensor composed of glucose oxidase and pistol-like DNAzyme. The glucose oxidase reacts with glucose to generate hydrogen peroxide, which were then used by the pistol-like DNAzyme for self-cleavage reaction. The cleaved fragment of DNAzyme is then detected by quantitative gel analysis after DNA electrophoresis.

Another approach is made by Gabriel et al (22). They developed a paper-based colorimetric tear glucose sensor with dimension of 24 mm x 10 mm. The sensor contains glucose oxidase and 3,3',5,5'-tetramethylbenzidine, so that the hydrogen peroxide generated by glucose oxidase could react with 3,3',5,5'-tetramethylbenzidine to turn blue. The tear fluid is collected with glass capillary tube and is transferred to the sensor paper. The sensor could detect as low as 50 μ M of glucose concentration.

1.3 Implantable drug delivery device for minimally-invasive drug therapy for diabetes mellitus

For drug therapies, various attempts were made to reduce pain associated with needed injections. There were studies conducted to identify the needle gauges and lengths that patients feel the least injection pain and anxiety (10). Long-acting formulations were developed to maintain glycemic control for a long

time with one injection (23, 24). However, these methods still could not resolve the fundamental problem of frequent and repeated needled injection, and for some medications, long-acting formulations could exhibit reduced drug efficacy (25). For this, implantable drug delivery devices were developed to replace needled injection drug therapy by delivering drugs from the internal reservoir after one-time implantation.

Intarcia developed a matchstick-sized osmotic pump, ITCA 650, for sustained delivery of exenatide, a short-acting GLP-1 RA (26). The pump contains exenatide sufficient for 6 months of delivery. The pump is implanted through 5 mm incision, and can be removed and replaced when the drug is depleted. Delpor has developed a titanium drug-eluting implant for sustained delivery of exenatide (27). The device is also small, 4 mm in diameter and 40 mm in length, and can be implanted between bicep and triceps muscle. The device is a hollow titanium cylinder without any mechanical actuator. There are two diffusion areas at two ends of the cylinder, where nano-pores are made to enable diffusion-based zero-order delivery.

For drugs such as insulin, post-prandial bolus delivery is important. Medtronic had developed a subcutaneously implanted insulin pump (Minimed 2007) that delivers insulin to intraperitoneal cavity through a silicone catheter (28). The pump is composed of a drug reservoir, an actuator, an antenna, a microelectronics and a battery. The pump is activated by an external controller through wireless communication. Lee et al., published a battery-less, magnetically-driven implantable pump for on-demand subcutaneous release of insulin (29). The pump could deliver a reproducible amount of insulin to achieve similar in vivo efficacy with injectable insulin.

1.4 Current limitations and research aims

Realization of minimally-invasive diagnosis and drug therapy for diabetes mellitus can be a huge benefit for diabetic patients who have to undergo countless painful experiences during chronic management of the disease. However, there are still unmet drawbacks of the aforementioned systems. Therefore, in this study, a minimally-invasive diagnosis methodology and a drug therapy methodology are developed to resolve the unmet drawbacks.

Tear glucose level exhibits high correlation to blood glucose level. In that sense, tear-based diagnosis can be a promising methodology for minimally-invasive diagnosis of diabetes mellitus. However, in current practices, the two-step measurement procedure, where the tear fluid is collected separately and is then transferred and loaded to the analytical instrument for measurement, can cause evaporation of samples and inaccuracy in measurements. This method is also inconvenient for patients: a relatively large volume of approximately 100 μl of tear fluid is often collected, which requires a long time of tear collection, as only approximately 6.5 μl of tear fluid is available at the preocular surface and the average rate of tear production is very low (1 $\mu\text{l}/\text{min}$) (30, 31). Moreover, tear fluid may be collected using a glass capillary tube or water-absorbing paper while monitoring with a slit lamp microscope by an ophthalmologist; however, this technique has not yet been fully proven to be appropriate due to its invasiveness to the eye when used by the patients themselves. Therefore, these conventional methodologies can still cause uncomfortable eye irritation or even damage and this can also lead to inaccurate measurements due to reflex tear production or an irrelevant increase in tear glucose due to the damaged tissue in the anterior surface of the eye (32-36). For this, a tear glucose sensor enabled

with concurrent tear collection and measurement is proposed, which can collect a small amount of tear fluid within 2 seconds and exert no damage to the eye. This will be introduced in chapter 2.

Currently developed implantable drug delivery devices for sustained delivery of drugs are advantageous in terms of small size and high patient acceptability. However, these devices cannot be adjusted with doses, turned on and off, or halted when needed. Therefore, these devices are not suitable for drug therapy that require bolus delivery, e.g. post prandial insulin delivery. The sustained delivery of GLP-1 RA with these devices is also suboptimal, because continuous activation of GLP-1 receptor can cause tachyphylaxis and reduce exenatide's ability to delay gastric emptying rate.

The implantable drug delivery devices for on-demand bolus delivery of drugs are capable of active interventions and multiple functionalities such as data transfer through telecommunication, thus enable optimal regimen of drug therapy. However, most of the devices contain batteries, circuit boards and mechanical actuators, so they are inevitably large in size. In addition, due to limited battery lifetime, patients have to undergo extraction surgery and re-implantation surgery to continuously benefit from these devices (37-39). In addition, the battery-less magnetic insulin pump possesses safety issue, as it could be accidentally actuated by a single household magnet, and a negative pressure built up in reservoir could reduce the amount of drug release. To resolve these issues, a small implantable magnetic pump actuated by a patterned magnetic field is developed, which could achieve minimally-invasive drug therapy with optimal regimen, semi-permanent use, and enhanced device safety. This will be discussed in chapter 3.

Chapter 2

Strip-type tear glucose sensor for concurrent tear collection and glucose measurement

2.1 Device design

In this work, a device for glucose measurement in tears (i.e., a tear-glucose device) is developed, meeting the following design criteria: for the convenience of the patients, the tear-glucose device needs to be equipped with both a tear-collector and a sensor as a single entity, thereby allowing for concurrent collection and measurement of tear fluids. In this device, a tip needs to be designed minimally-invasive as it must be in contact with the preocular surface (i.e., an ocular tip). Tear collection should be conducted for a short time, hence resulting in a small volume of collected tear fluid. The sensor also needs to be sensitive enough to accurately measure glucose concentrations in a small quantity of tears. At the same time, a concept of device design that could be quick to apply to clinical applications and easy to manufacture is also proposed.

To prepare such a tear-glucose device, an assembled entity consisting of a lid and a strip-type glucose sensor was designed. The lid was engineered to consist of a minimally-invasive ocular tip and a hollow body with a slit, where the strip-type glucose sensor could be inserted for tight assembly. In the ocular tip, a micron-size inlet was prepared, where after its contact with the preocular surface, a tear could be absorbed and delivered to reach the sensor inserted in the lid. For the strip-type glucose sensor, a commercially-available test strip (Accu-Chek Performa, Roche Diagnostics, Switzerland) was employed, which is known to measure glucose levels via electrochemical means with high accuracy and selectivity (40). However, in this work, this test strip was modified to be suitable specifically for the collection and measurement of a small quantity of tear fluid. Therefore, the lid herein possessing a simple structure would not be difficult to manufacture. The glucose test strip has been already widely used in clinical settings and thus, its manufacturing process is already well developed for a large-scale production.

The tear-glucose device herein was first tested at the range of physiological glucose concentrations present in tears under *in vitro* simulated environments. To test *in vivo* usability, the device was placed in contact with the inferior palpebral conjunctiva (IPC) of rabbit eyes to collect and measure tear fluids, since the IPC can be considered less sensitive compared with other regions in the preocular space (41). The correlation between glucose concentrations measured in blood and tears were also validated. After application of the device, the IPC tissue was also examined for the purpose of safety evaluation.

2.2 Methods

2.2.1 Lid

The lid was prepared to serve as an interface between the eye surface and glucose sensor to safely collect and deliver tear fluids. To achieve this, the lid was first designed to consist of two distinct parts: the ocular tip and the hollow body using SolidWorks (Dassault Systèmes SOLIDWORKS Corp., USA). As shown in Fig. 2.1, the ocular tip was shaped to be circular (2 mm in diameter) with rounded boundaries, which has been reported to not damage the IPC tissue during contact according to a previous study (42). In the ocular tip, a small inlet (1 x 0.5 x 0.4 mm, W x H x L) was prepared to be able to absorb tear fluids via capillary action after contact with the IPC and to minimize the dead volume of tear fluid trapped inside of the inlet. The hollow body was designed to possess a slit (7.4 x 0.55 mm, W x H) for insertion of the strip-type glucose sensor used herein. The opening (1 x 1 mm, W x H) was also made at the top of the hollow body so that tear fluids could be smoothly absorbed and transferred to the glucose sensor. Fig. 2.2 shows the lid fabricated with a 3D printer (ProJet 3500 HD, 3D Systems, USA), using the printing material Visijet M3 Crystal, certified by USP (United States Pharmacopeia) Class VI.

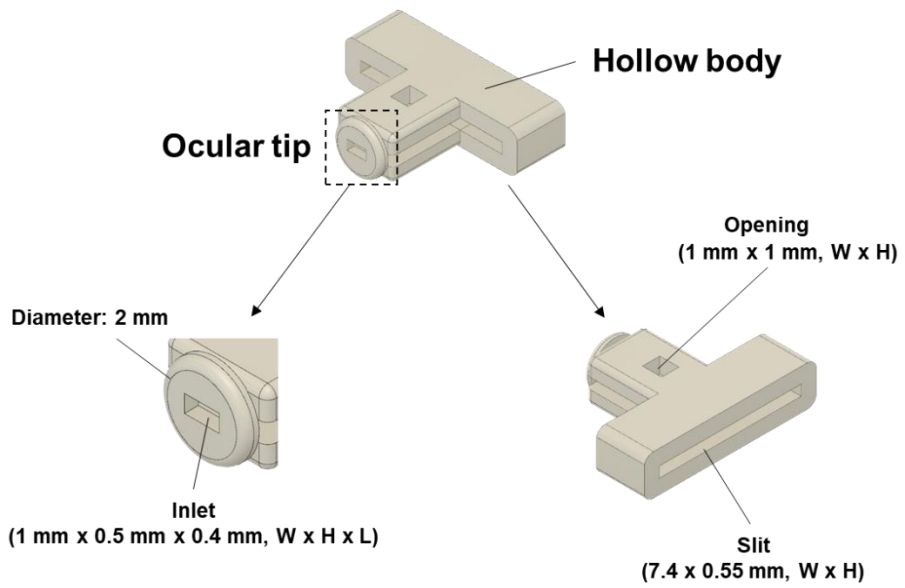


Figure 2.1 Schematic images of the lid for minimally-invasive tear collection

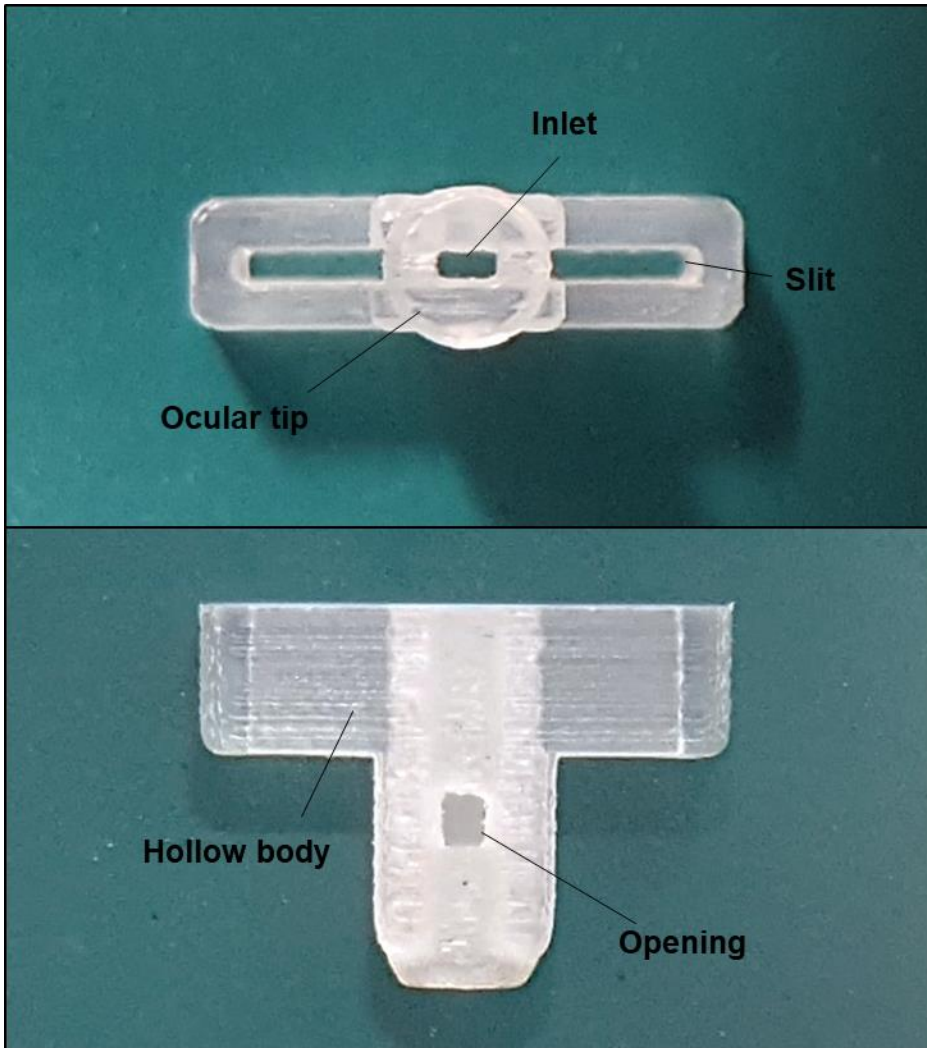


Figure 2.2 Optical images of the lid for minimally-invasive tear collection

2.2.2 Strip-type glucose sensor

To prepare a strip-type sensor, the commercially available Accu-Chek test strip was employed and modified for the purpose of glucose measurement in tears. This test strip was equipped with an electrochemical sensor with a low limit of quantification ($< 45 \mu\text{M}$) and high selectivity for glucose measurement (43). In this sensor, collecting a fixed volume of fluid sample is important for accurate measurement of glucose, as the electrical current that varies according to the rate of glucose oxidation is also influenced by the volume of fluid in the reaction chamber. The Accu-Chek test strip is originally designed to measure glucose levels in the blood, and thus the reaction chamber with the electrodes is shaped to hold $0.8 \mu\text{l}$ of fluid.

In this work, it was attempted to minimize the volume of collected tear fluid, so the test strip was modified to decrease the volume of the reaction chamber. During this process, the major electrodes for glucose measurement needed to be kept intact. In the reaction chamber of the Accu-Chek test strip, four different electrodes were embedded; the counter, reference, working and fill-sufficiency electrodes. For glucose measurement, the counter, reference and working electrodes must be kept intact. However, the fill-sufficiency electrodes for detection of the presence of liquid might not be necessary to test the prototype device prepared in this work. Given these facts, as shown in Fig. 2.3, the frontal end of the strip was cut out to the extent where the counter, reference and working electrodes were not affected, to reduce the length of the reaction chamber. The sharp edges in the frontal end were also rounded off to avoid possible damage to the IPC tissue. Then, the other end of the reaction chamber was punched out, removing the fill-sufficiency electrodes, to further reduce its

volume. Thus, after modification, the resulting strip-type glucose sensor became equipped with a reaction chamber containing a volume reduced by half to 0.4 μl .

2.2.3 In vitro evaluation

A glucose solution was prepared by dissolving D-(+)-Glucose (Sigma-Aldrich, USA) at the concentrations of 0, 0.01, 0.05, 0.1, 0.2, 0.4 and 0.8 mM in phosphate-buffered saline (PBS) at pH 7.6, respectively. To collect 0.4 μl of the glucose solution, the ocular tip of the device was placed in contact with the glucose solution for 2 s. For measurement of the concentration of glucose, the tear-glucose device was connected to a potentiostat (DY2113, Digi-Ivy, USA) to apply 150 mV and the output current was obtained using the amperometric i-t curve mode.

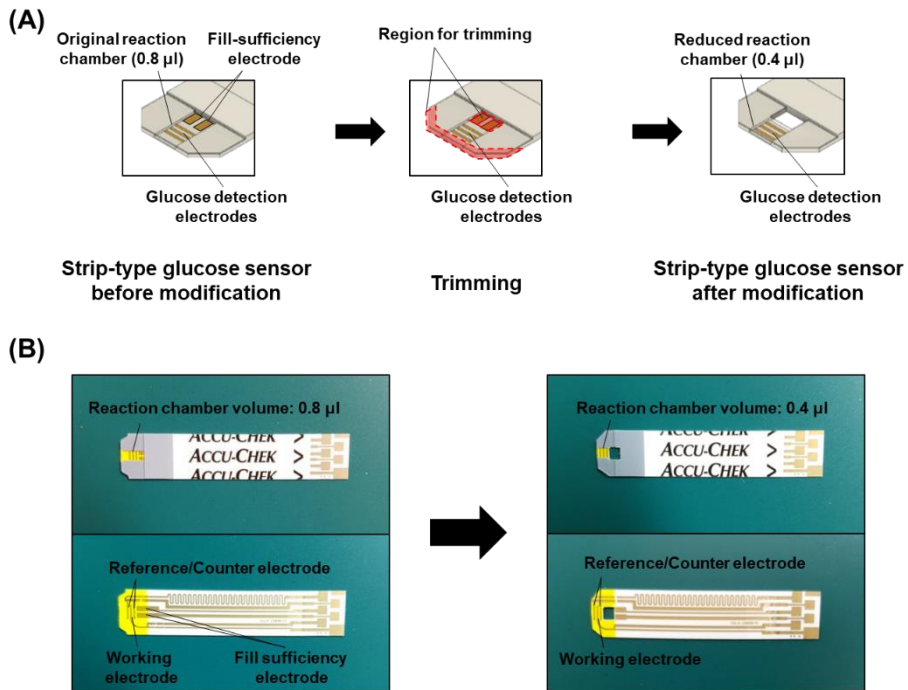


Figure 2.3 Modification of strip-type glucose sensors. (A) Schematic description of sensor modifications to reduce the volume of the reaction chamber. (B) Optical images of the strip-type glucose sensors before and after modification, showing the embedded electrodes and circuits.

2.2.4 In vivo evaluation

Approval for the in vivo experiments was granted by the Institutional Animal Care and Use Committee (IACUC No. 15-0285) at the Biomedical Research Institute of the Seoul National University Hospital. All experiments were performed in accordance with relevant guidelines and regulations. Male New Zealand white rabbits (2.5~3.0 kg) were raised in a controlled environment (temperature: 21 ± 1 °C, humidity: 55 ± 1 %, light/dark cycle: 12 hours, and food and water ad libitum). Hyperglycemia was induced in animal models via anesthetization, as reported in previous studies 13,14,28. To achieve this, the rabbits were first anesthetized with a subcutaneous injection of a cocktail of 15 mg/kg ketamine (Ketamine: Yuhan, Korea) and 5 mg/kg xylazine (Rompun: Bayer, Germany) and after 40 min, a booster shot of 7.5 mg/kg ketamine and 2.5 mg/kg xylazine was given. The glucose concentrations in both blood and tears were measured at 15, 30, 45, and 60 min after the first shot of the anesthetics. To measure blood glucose concentrations, blood was drawn from the right ear vein of the rabbit using a lancet, and a glucometer was used (Accu-Chek Performa, Roche Diagnostics, Switzerland). To measure the tear glucose concentrations, the lid of the tear-glucose device connected to a potentiostat was in contact with the IPC of the rabbit eyes for 2 s. At the specified endpoints of the experiments, the presence of tissue damage on the IPC surface was examined, following a previously reported protocol 31. Briefly, a 5- μ l drop of 0.25 % w/v fluorescein sodium solution was instilled in the eye and after 5 min, the eye was washed thoroughly with normal saline to remove excess fluorescein solution. Then, a fluorescent image of the IPC surface was obtained, using a camera (Galaxy S7, Samsung, Korea) equipped with excitation (475 nm) and emission (542 nm) light filters (Thorlabs, USA).

2.2.5 Statistical analysis

Statistical analysis was performed with two-tailed Pearson's correlations using SPSS (SPSS version 23, IBM, USA). A Student's t-test was performed to obtain the P values. $P < 0.05$ was considered a statistically significant difference.

2.3 Results

2.3.1 Tear-glucose device

The tear-glucose device herein described was prepared by simple assembly of the lid and the modified strip-type glucose sensor, as shown in Fig. 2.4. After insertion in the slit, the strip-type sensor was tightly fit, and the reaction chamber was properly aligned to the inlet prepared in the ocular tip of the lid. After that, the counter, reference and working electrodes were each connected to the counterpart connection in a potentiostat to apply 150 mV of DC voltage and measure the electrical current. In this work, a two-electrode system was used and thus, the counter and reference electrodes were connected as a single cathode while the working electrode was connected separately as an anode.

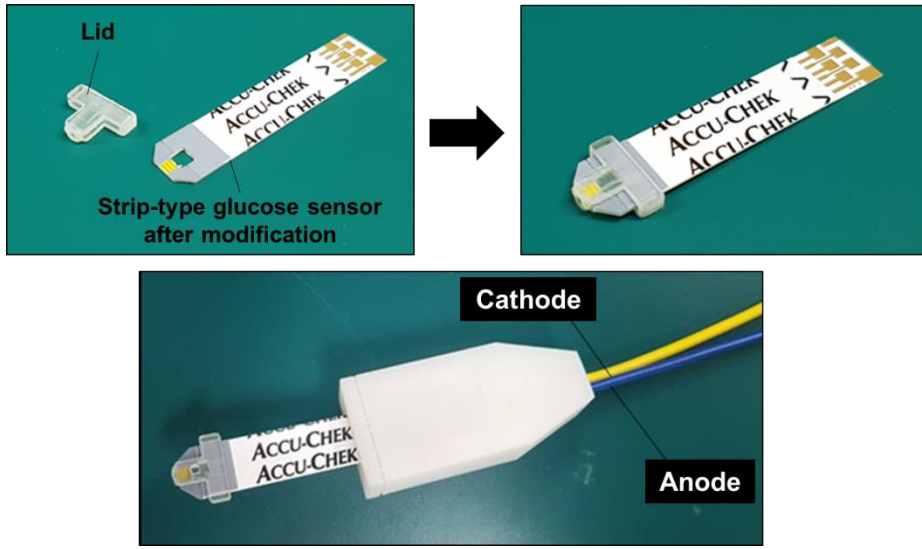


Figure 2.4 Preparation of the tear-glucose device. The modified strip-type glucose sensor and the lid are assembled and connected to the potentiostat. The counter and reference electrodes were connected together as a single cathode and the working electrode worked as an anode.

2.3.2 In vitro performance evaluation

To test the feasibility of the tear-glucose device herein, in vitro calibration was conducted with a glucose solution prepared in phosphate-buffered saline (PBS) with varying concentrations of 0, 0.01, 0.05, 0.1, 0.2, 0.4 and 0.8 mM. As shown in Fig. 2.5, a highly linear relationship was obtained between the glucose concentration and electrical current ($R^2 > 0.9864$), indicating that the tear-glucose device herein described was valid to measure the in vivo glucose concentration in tear fluid, which was reported to range from 0 ~ 0.6 mM (44).

2.3.3 In vivo performance evaluation

To evaluate the feasibility of the tear-glucose device herein described, in vivo experiments were conducted using rabbits, where the blood glucose concentration was elevated through anesthetization (14, 20, 44). In this work, the tear glucose concentrations were measured with the tear-glucose device and the blood glucose concentrations were measured with a blood glucometer approved for clinical use (Accu-Chek Performa, Roche Diagnostics, Switzerland) at scheduled times of 15, 30, 45, and 60 min after anesthetization.

Fig. 2.6 shows the plot of the tear and blood glucose concentrations obtained from all eight rabbits, showing a linear relation. However, the data points were spread and hence the linear correlation appeared not to be very strong ($R^2 = 0.7640$, $df = 30$, $P < 0.05$). This discrepancy was observed in previous reports and was ascribed to the inherent differences among tested animals (14, 20). Therefore, when the data points averaged at each time of measurement (i.e., at every 15 min) were plotted (14), as shown in Fig. 2.7, a strong linear correlation with a statistical significance was obtained ($R^2 = 0.9617$, $df = 2$, $P < 0.05$).

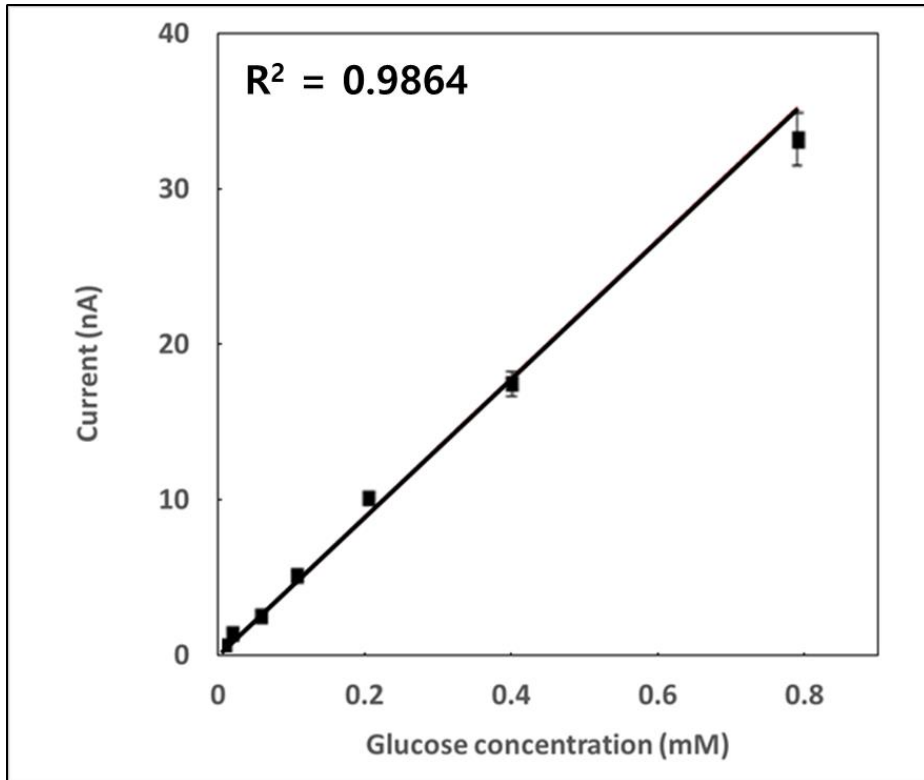


Figure 2.5 Calibration curve for varying glucose concentrations obtained with the tear-glucose device.

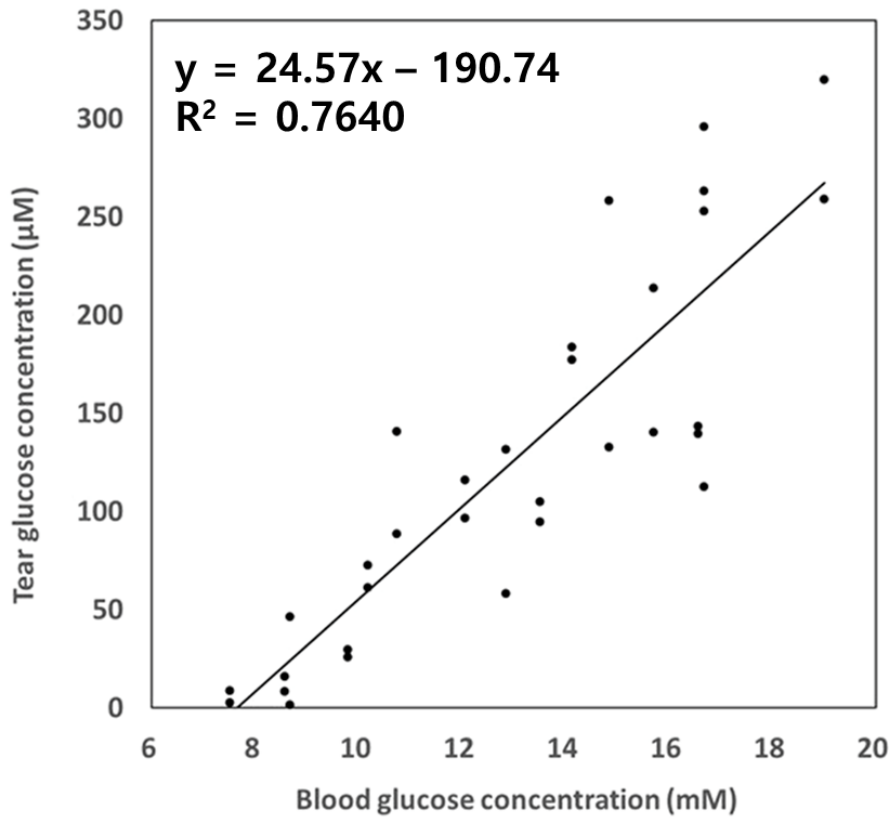


Figure 2.6 Correlation between blood glucose concentrations and tear glucose concentrations obtained with the tear-glucose device from all eight rabbits (i.e., eight eyes) employed in this work.

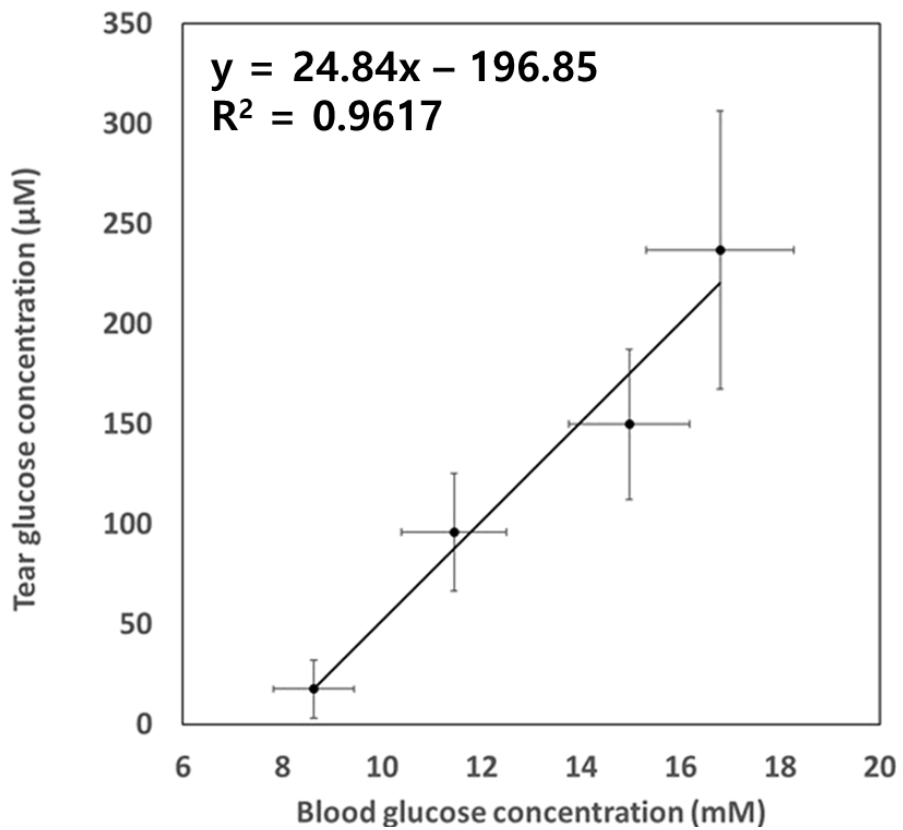


Figure 2.7 Correlation between average glucose concentrations in tear and blood obtained at each scheduled time of measurements.

In this study, it was sought to show that the tear-glucose device herein described can estimate the blood glucose concentration based on the glucose concentration measured in tears. To evaluate this, the estimated and actual blood glucose concentrations were plotted in a Clarke error grid (45, 46). The estimated blood glucose concentrations were calculated from the tear glucose concentrations using the equation obtained from the graph in Fig. 2.7. The actual blood glucose concentrations were measured from the blood using a glucometer approved for clinical use. As shown in Fig. 2.8, all data points are in the zones A and B, suggesting that the blood glucose concentrations estimated with the tear-glucose device herein are highly correlated and possibly interchangeable with those conducted with the conventional blood glucose measurement method. Approximately 65.6 % of the data points are in the zone A, implying a relatively higher accuracy of blood glucose measurement with the tear-glucose device described herein.

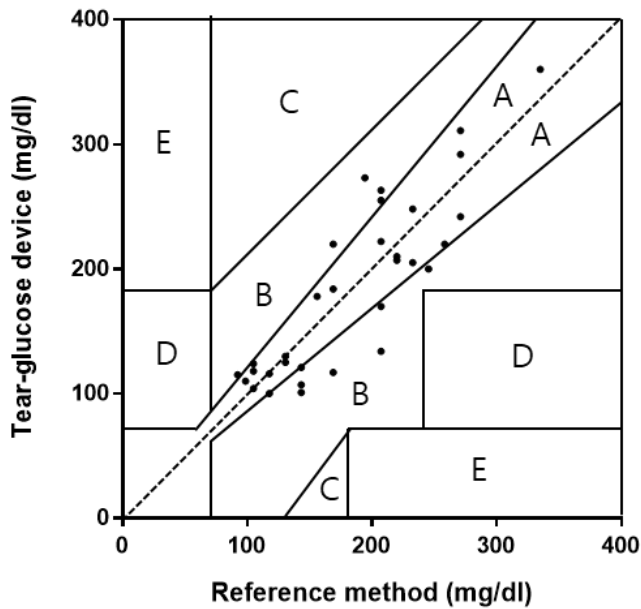


Figure 2.8 Clarke error grid analysis on blood glucose concentrations obtained with the tear-glucose device and a clinically approved glucometer.

All data were plotted within zones A and B, showing the reliability of the blood glucose concentrations estimated with the tear-glucose device. The y-axis represents the blood glucose concentration estimated from tear glucose concentration measured with the tear-glucose device, and the x-axis represents the blood glucose concentration measured with a reference method using a commercially available glucometer. Region A indicates that the data are within 20% error from the reference method. Region B indicates that the values are over the 20% error mark, but do not imply an inappropriate treatment. Region C indicates that the data will lead to an unnecessary treatment. Region D indicates that the data will fail to diagnose hyperglycemia or hypoglycemia. Region E indicates that the data will lead to a treatment for hypoglycemia to a patient with hyperglycemia, or vice versa.

2.3.4 In vivo safety evaluation

To evaluate the safety of the tear-glucose device, the IPC tissues was examined at the end point of the experiments, i.e., after each of the four times of contact of the tear-glucose device on the IPC, where the eye surface was stained with a fluorescein solution to assess possible tissue damage (47). As shown in Fig. 2.9, after contact of the tear-glucose device, the IPC tissues were not observed to be stained, as seen with the non-treated, negative control eye, indicating no epithelial tissue damage. In contrast, when the IPC was in contact with a glass capillary tube, conventionally used for tear collection, an apparent sign of staining was observed due to damage of the IPC tissue.

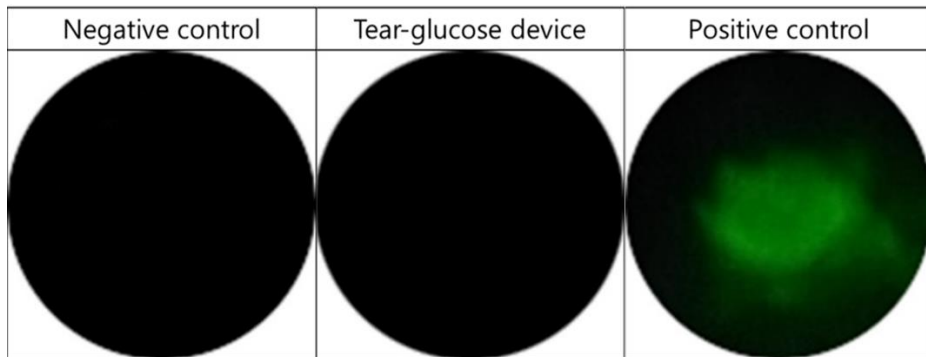


Figure 2.9 Representative fluorescent images obtained from the IPCs of fluorescein-stained rabbit eye. For the negative control group, no treatment was applied to the IPC. For the tear-glucose device group, the tear-glucose device was applied to the IPC four times at intervals of 15 min during 60 min. For the positive control group, a glass capillary tube was placed in contact with the IPC once.

2.4 Discussions

Tear glucose measurement has been suggested as a potential methodology of minimally-invasive blood glucose prediction (32, 48, 49). Most of the previous studies focused on developing sensors with a higher accuracy since the glucose concentration in tears is known to be lower than that in the blood (14, 15, 50). However, the studies on devices for practical, self-diagnostic applications is scarce. In this context, a device with a novelty of allowing concurrent tear collection and glucose measurement could be useful and convenient for users. Such a device would be more advantageous if the measurement could be reliable even with a small quantity of tear fluid as this would allow for a short time of tear collection, hence less invasiveness on the precocular tissues.

Therefore, the tear-glucose device was proposed herein as a minimally-invasive self-diagnostic tool for prediction of blood glucose levels. The lid in the device was shown to not damage the eye tissues due to its design with a proper contact area and rounded boundaries without sharp edges (Fig. 2.9) (42). Although the lid herein was made of a slightly hydrophobic material (Visijet M3 Crystal, 3D Systems, USA), the micron size inlet still allowed for a strong capillary pressure, hence safe and efficient absorption of tear fluid, which could be rapidly transferred to fill the reaction chamber with a reduced volume (0.4 μl) in the strip-type glucose sensor (Fig. 2.3). With a lid made of a more hydrophilic material, it is expected that a more amount of tear can be collected in a more efficient manner (51). Since the lid for tear collection and the strip-type sensor for measurement were assembled as a combined entity, the glucose concentration could be measured almost instantaneously after tear collection without its evaporation. Therefore, the whole process from tear collection to

measurement took less than 2 seconds in this work. This short time of preocular contact would minimize eye irritation and possible measurement errors caused by reflex tear generation (14, 32, 36). For measurement, a 150 mV was applied to induce an electric current at 300 nA. Considering the maximum preocular contact time of 2 s, this would give at most 110 nJ, which is far less than that known to be safe when applied to the ocular tissues (12 J) (52, 53).

The *in vivo* findings revealed that the glucose concentrations in tears measured with the tear-glucose device were highly correlated with those in blood measured with a glucometer in clinical use Fig. 2.6. This correlation was more prominent when the relations were plotted using the average glucose concentrations obtained at each measurement time Fig. 2.7. Those results suggested that the tear-glucose device herein could have a similar level of accuracy compared to a conventional glucometer (Fig. 2.8) and compared to the methodologies reported in previous studies (14, 20). However, due to an inherent variation among individuals, as well as the presence of temporal correlation between the blood and tear glucose levels (Fig. 2.10), there could be some limitations for treating accurate glycaemia events with the diabetic patients. In this sense, the device could be better suited for healthcare purposes, especially for measurement of fasting glucose concentration in the morning or blood glucose at night, or early diagnosis of pre-diabetes mellitus. With ease of use and minimal invasiveness, the device herein could be more favored by the people with a high chance of getting diabetes mellitus, allowing for watching the blood glucose level early without much of discomfort even under a healthy condition. Considering actual applications in human clinical settings, a strip-type electrochemical sensor with a higher sensitivity may need to be developed. For humans, the tear glucose concentrations may vary according to the tear

collection methods, but are approximately 50 times lower than those in blood (54, 55) and this dilution factor was lower than that reported in rabbits (25 times) (44). However, the device herein was able to measure the glucose concentrations at such lowered ranges expected in human tear fluids (Fig. 2.11).

However, the tear-glucose device is expected to have limitations in measuring the tear glucose concentration in hypoglycemia. The blood glucose concentration lower than 4 mM is considered hypoglycemic. According to Peng et al., tear glucose corresponding to the blood glucose at 2~4 mM is reported to be 0.01~0.03 mM (20). Although the tear-glucose device could measure the tear glucose concentration at 0.01 mM in vitro, the limit of quantification (LOQ) suggested by the glucose sensor was 0.045 mM, implying that the measurement of tear glucose in range of 0.01~0.03 mM could be inappropriate. Therefore, a sensor with lower LOQ should be implemented to the current design to measure the tear glucose concentration at hypoglycemic blood glucose concentration.

Another consideration would be the influence of sensor lot number to the calibration curve between the glucose concentration and the electric current. The glucose sensor employed herein is designed to have different calibration curve for difference lot number. Although the sensors used in this study shared the same lot number (lot number: 475404), if a new lot of sensors are to be used, a new calibration curve should be obtained.

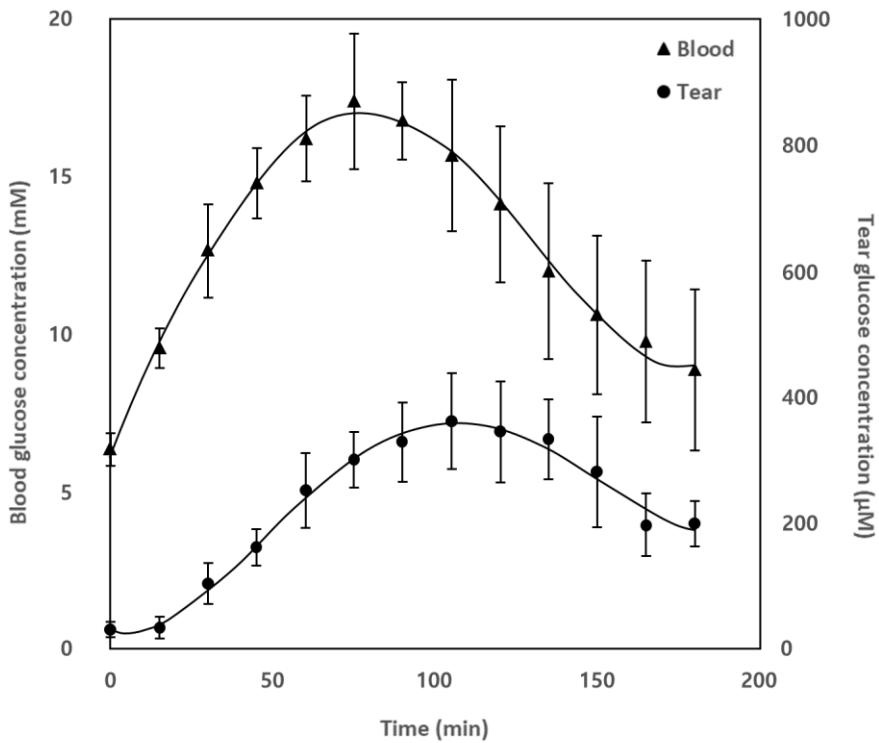


Figure 2.10 Temporal correlation between blood and tear glucose concentrations, which were measured by a glucometer and tear-glucose device herein, respectively. To increase the blood glucose level, rabbits (n = 6) were anesthetized with a single, subcutaneous injection of a cocktail of 15 mg/kg ketamine and 5 mg/kg xylazine and they were left without boosters to decrease the blood glucose level afterwards. Both blood and tear glucose concentrations were measured every fifteen minutes after anesthetization. The results revealed that a lag time was indeed present between the profiles of blood and tear glucose concentrations, as reported in previous studies (32, 44), which implied an acceptable accuracy of the tear-glucose device prepared in this work.

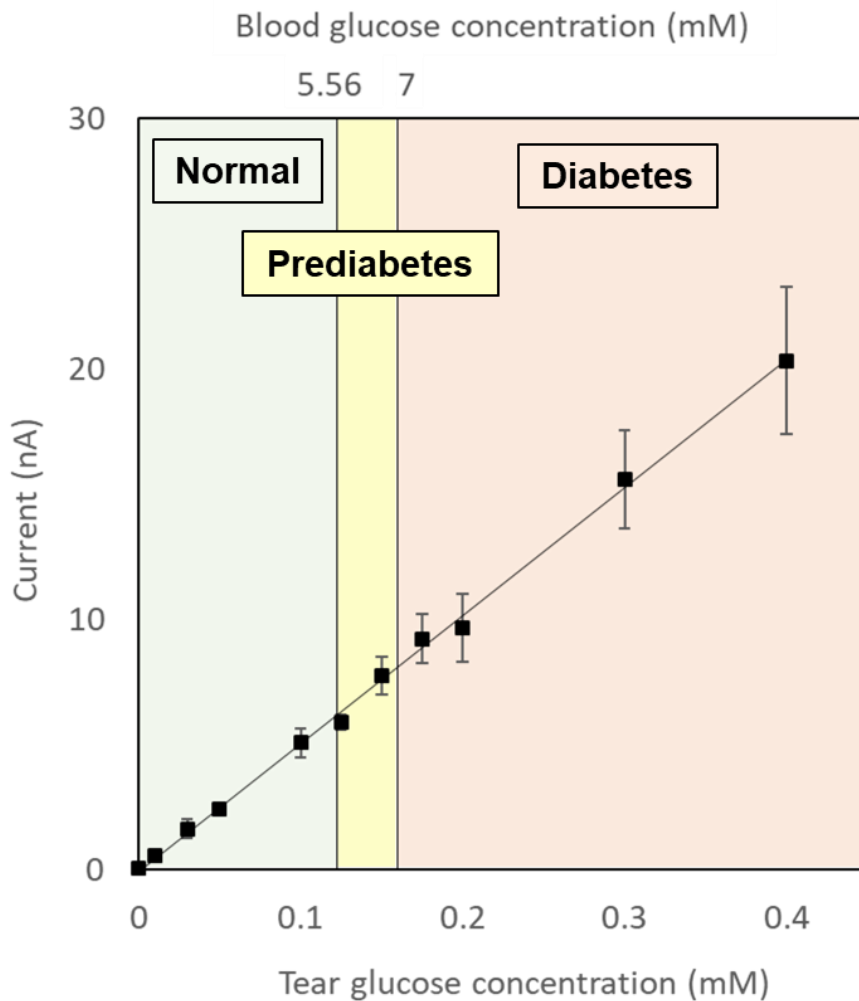


Figure 2.11 Device evaluation at the range of glucose concentration in human tear fluids. Tear-glucose device developed herein was able to measure the glucose concentrations at the ranges of 0.03 – 0.12 mM, 0.12 – 0.16 mM, and 0.16 mM to higher, which were expected to be present in human tear fluids under the normal, pre-diabetic and diabetic conditions, respectively.

Chapter 3

Implantable magnetic pump for bolus delivery of exenatide

3.1 Device design

For an optimal regimen of exenatide with better patient compliance, an implantable pump capable of on-demand and bolus infusion would be advantageous (37-39). For this, a battery-less, implantable pump enabled with magnetic actuation (i.e., the magnetic pump) was proposed in a previous study (29). After implantation, the prototype of the magnetic pump reproducibly delivered an accurate amount of drug only when the magnet was applied outside the skin noninvasively. With a refill port in the pump and without the need of a battery for infusion, an implanted magnetic pump was envisioned for semi-permanent use without replacement surgery.

In this work, a pump actuated via a magnetic force for exenatide delivery is proposed to maintain the advantages of the pump designs in the previous work.

Especially due to the relatively short half-life of exenatide, the regimen of on-demand and bolus infusion could closely follow postprandial secretion of GLP-1 in normal physiology. However, the magnetic pump proposed herein was extensively improved compared to the previous design, considering safety, reproducibility, and longevity. The magnets for actuation were embedded in a specific pattern like a key and key-hole to prevent unintentional actuation possibly caused by a general household magnet. The reservoir for exenatide was composed of a flexible biomaterial to avoid negative pressure build-up by drug consumption via multiple infusions, thereby prolonged longevity after implantation and drug-dose reproducibility with less frequent refill procedures. The pump was also equipped with two distinct check-valves to better prevent any possible infiltration of bodily fluid into the pump.

First, the performance of the upgraded magnetic pump was assessed for exenatide infusion under *in vitro* environments. For the evaluation of *in vivo* efficacy, Goto-Kakizaki (GK) rats were employed, which are a non-obese T2D animal model that spontaneously develop hyperglycemia due to progressive pancreatic β -cell failure (56). Envisioning clinical applicability, the pharmacokinetic and pharmacodynamic profiles of the implanted pump were compared with those treated with conventional, subcutaneous (SC) injections of exenatide of the same dose and administration schedule. For pharmacodynamic evaluation, the body weight, food intake, glucose tolerance and gastric emptying were investigated, as well as pancreatic β -cells and adipocytes in the visceral fat (57-59).

3.2 Methods

3.2.1 Materials

Exenatide (MW = 4187 Da) was purchased from Cosmogenetech (Korea). Phosphate buffered saline (PBS) and formalin were purchased from Thermo Fisher Scientific (USA). Acetonitrile (ACN) and methanol were purchased from Daejung (Korea). D-glucose, fluorescein, trifluoroacetic acid (TFA) and paracetamol were purchased from Sigma (USA). Betadine was purchased from Firson (Korea). Accu-chek Performa glucometer, Accu-chek Performa blood glucose test strips, and lancets were purchased from Roche Diagnostics (Switzerland). Exenatide enzyme immunoassay (EIA) kit was purchased from Phoenix Pharmaceuticals (USA). Rat insulin ELISA kits were purchased from Crystal Chem (USA). Goat anti-rabbit IgG-HRP antibody was purchased from Santa Cruz Biotechnology (USA). Rabbit anti-rat insulin antibody was purchased from Cell Signaling Technology (USA). Vector NovaRED Peroxidase (HRP) Substrate kit was purchased from Vector Laboratories (USA).

3.2.2 Magnetic pump fabrication

The structure of the magnetic pump was drawn using a 3D modeling software (SolidWorks, Dassault Systèmes, France), and each of the constituent components was manufactured with FullCure720 (Objet Geometries, Israel) using a 3D printer (Eden 350 V, Objet Geometries, Israel). A plunger was fabricated by embedding four M_P magnets (diameter: 5 mm; thickness: 1 mm) with patterned polarities. In a barrel, four M_B magnets (diameter: 3 mm; thickness: 1.5 mm) were embedded with a pattern reciprocal to those of M_P . A refill septum made of polyurethane rubber and a 3D printed refill port (inner

diameter: 2.2 mm; outer diameter: 3.4 mm) was inserted for connecting to a drug container. To fabricate a fluid conduit, two check valves (Minivalve, Netherland) were connected at the ends of the silicone tube (inner diameter: 1.6 mm; outer diameter: 1.8 mm). A flexible drug container was made in the shape of a bag using a 100- μ m thick polyurethane membrane (Nihon Matai, Tokyo, Japan). Top and bottom films were each made by pressing the polyurethane membrane with the molds, which were then bonded with an adhesive (Vetbond, 3M, USA) to produce a hollow drug container. All constituent components were assembled and bonded firmly with a medical adhesive (Vetbond, 3M, USA). The final pump was coated with Parylene C by chemical vapor deposition for better biocompatibility (60). The detailed fabrication procedure is depicted in Fig 3.1. The total volume of the magnetic pump was approximately 7.82 ml (36.0 mm \times 20.7 mm \times 10.5 mm, $l \times w \times h$) with 0.6 ml for the drug container. To prepare an external device, a rotatable head was first prepared, which was embedded with four magnets (diameter: 5 mm; thickness: 5 mm) with a distinct polarity pattern. Then, the rotatable head was loosely assembled with a device body, on top of which a cap was attached. Thus, when the external device is approached to the implanted pump, the rotatable head can rotate to align the patterned M_E and M_P and pull the plunger.

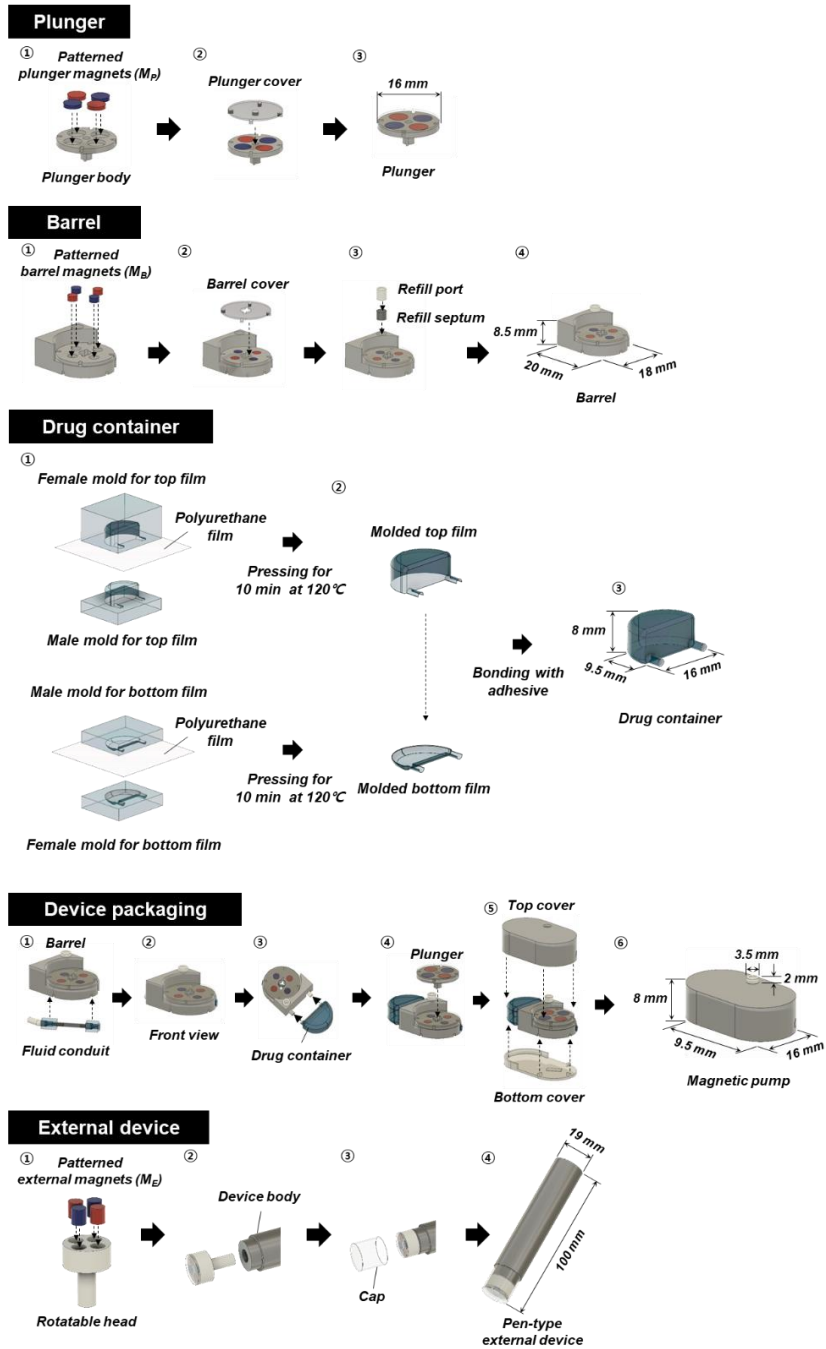


Figure 3.1 Detailed description of the magnetic pump fabrication procedures.

3.2.3 Magnetic design principles

To find a proper design for actuation with the magnets in the pump, the attraction forces between M_B and M_P , and M_P and M_E were measured with a load cell (ULC-1N, Interface, USA). The distances between two magnets were set at 1 and 4.5 mm for M_B and M_P , and M_P and M_E , respectively, considering their location in the pump. The measurement was performed in triplicate. The attraction force between M_P and M_E , was measured to be 0.62 ± 0.02 N, which was larger than the force between M_B and M_P (0.26 ± 0.04 N). Therefore, the external device with M_E can overcome the attraction between the plunger and barrel, and lift the plunger in the pump.

3.2.4 High-performance liquid chromatography measurements

To evaluate the pump performance and stability of exenatide, the concentration of exenatide in PBS was measured by high-performance liquid chromatography (HPLC) (1260 series, Agilent Technologies, USA) equipped with a C18 column ($5 \mu\text{m}$, $4.6 \text{ mm} \times 250 \text{ mm}$; Agilent Technology, USA) (61). The mobile phase was made with a mixture of ACN with 0.1% TFA (ACN/TFA) and an aqueous solution of 0.1% TFA (DI/TFA). The mobile phase was pumped at a flow rate of 1 ml/min in gradient mode, in which the volume ratio of ACN/TFA:DI/TFA was shifted from 40:60 to 50:50 for 25 min. The injection volume of the sample was 10 μl and the exenatide concentration was measured at 215 nm.

3.2.5 In vitro performance test

The magnetic pumps used in in vitro performance tests were loaded with an exenatide solution (6.28 mg/ml) and were fully immersed in pH 7.4 PBS at 37°C. To evaluate the drug release profile, the pumps were actuated with the

external device with patterned magnets for thirty times ($n = 3$). The drug concentration was measured every five times of actuation with HPLC. For safety assessment, the pumps were actuated thirty times with a magnet (0.3 T) with single polarity ($n = 3$). The long-term drug release profile was determined by actuating the pumps and measuring drug concentration at day 1, 8, 15, 22, 29 ($n = 5$). To assess any possible leakage from the pump, pumps were left for 4 weeks in PBS without actuation ($n = 5$). To evaluate influences of drug replenishment on drug release profile, the magnetic pump loaded with exenatide (6.28 mg/ml) was actuated three times before and after a replenishment procedure while being fully immersed in pH 7.4 PBS ($n = 3$).

3.2.6 Accelerated depletion test

For this test, the magnetic pump loaded with a 1 mg/ml fluorescein solution was fully immersed in pH 7.4 PBS at 37°C and actuated consecutively up to 320 times until depletion. Right after the actuation of interest, the medium was collected and measured with a UV-Vis spectrophotometer (UV-1,800, Shimadzu, Japan) at a wavelength of 488 nm to obtain the cumulative amount of fluorescein release.

3.2.7 Stability evaluation of exenatide

An exenatide solution (6.28 mg/ml) was loaded in the flexible drug container used for the magnetic pump ($n = 3$) and stored in 37°C for 28 days, the stability of which was analyzed by comparing that of a fresh solution of exenatide (day 0) by using HPLC and circular dichroism (CD) spectroscopy (Applied Photophysics, UK). For CD spectroscopic analyses, an exenatide solution, either from a fresh solution or after incubation in the pump herein, was placed

in a quartz cuvette (Hellma Analytics, Germany) with a 0.2-mm path length and the CD spectra were obtained by scanning at a range of 190–260 nm.

3.2.8 Animal study

For in vivo pharmacokinetics test, ten-week old, female Wistar rats (Orient Bio, Korea) weighing 200 – 250 g were employed. Wistar rats were used instead of Goto-kakizaki (GK) rats to avoid anti-exenatide antibody formation. The anti-exenatide antibody was reported not to affect the efficacy of exenatide; however, it was reported to influence quantification of exenatide using ELISA kit. The animals were divided into two groups: Pump-Ex group (n = 5): animals implanted and treated with the magnetic pump loaded with exenatide and Inj-Ex group (n = 5): animals treated with the SC injection of exenatide.

For in vivo pharmacodynamics test, ten-week old, male GK rats (Japan SLC, Japan) were employed, weighing 200 – 250 g. The animals were divided into four groups: 1) Pump-Ex group (n = 5) and 2) Inj-Ex group (n = 5). 3) Pump-PBS group (n = 4), and 4) Inj-PBS group (n = 4). The pump implantation procedure is depicted in Fig. 3.2. For all groups, the same volume of exenatide solution or PBS without exenatide was administered twice per day for 7 weeks, respectively and their pharmacokinetic and pharmacodynamic profiles were compared (Fig. 3.3). No outliers were excluded from the data analysis. All surgical and experimental procedures used in the present study were approved by the Animal Care and Use Committee at Seoul National University (approval #: 17-0210-S1A0). The animals were housed in a specific pathogen-free facility with controlled temperature, humidity, and 12:12 h light/dark cycle. Standard chow diet and water were provided ad libitum during the experiments.

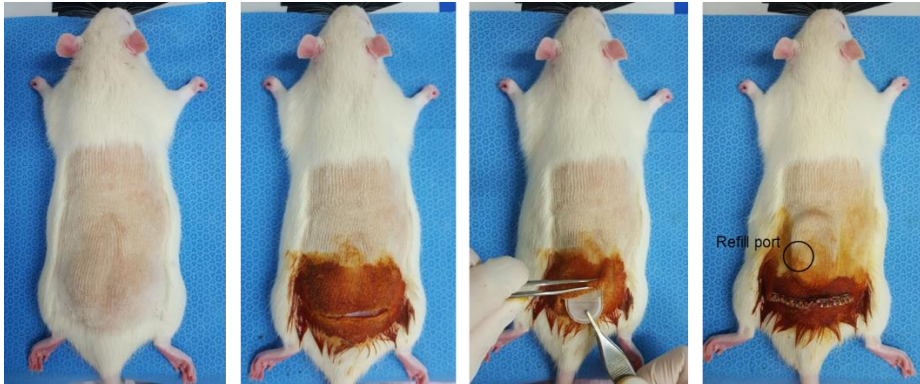


Figure 3.2 Surgical procedure for the magnetic pump implantation and exenatide replenishment. A GK rat was anesthetized via isoflurane inhalation and the dorsal area was shaved. After sterilization with betadine, the dorsal skin was incised at about 3 cm. The magnetic pump was implanted into the subcutaneous pocket. The wound was closed using surgical clips (9 mm Autoclips, MikRon Precision, USA) and disinfected with betadine.

- Groups: Pump-Ex, Pump-PBS, Inj-Ex, Inj-PBS

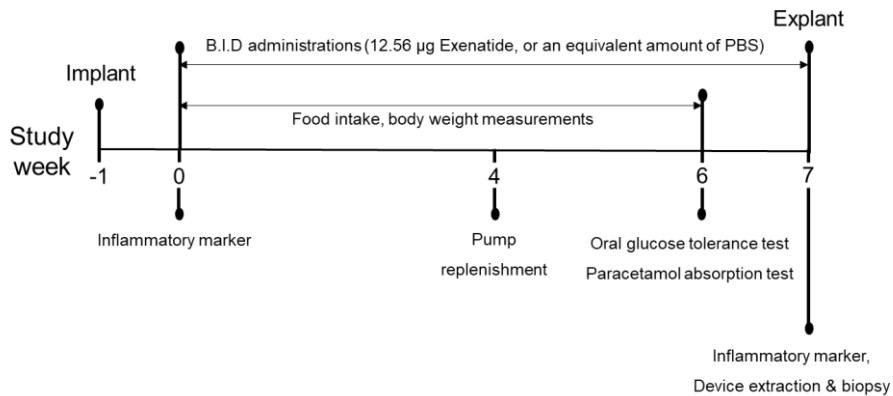


Figure 3.3 Timeline of the study events. For the Pump-Ex and Pump-PBS groups, one week prior to the experiments, rats underwent a surgical procedure to subcutaneously implant the magnetic pump. Over the experiments, the animals received two administrations per day at 9:00–10:00 h and 17:00–18:00 h, respectively, every day for 7 weeks. Thus, for the Pump-Ex and Inj-Ex, the same-dose exenatide (12.56 µg in 0.1 ml) was administered by pump actuation and SC injection, respectively. For the Pump-PBS and Inj-PBS, an equivalent volume of PBS (0.1 ml) was administered by pump actuation and SC injection, respectively. Body weight and food intake were monitored three times a week.

3.2.9 Glucose tolerance test

After 6 weeks of treatment, the oral glucose tolerance test (OGTT) was performed with all animal groups. An oral gavage with D-glucose (2 g/kg) was given to a rat after fasting overnight. The blood glucose level was measured at 0, 15, 30, 60, 120 and 180 min via a tail vein, using a glucometer. At the same scheduled times, a blood sample was withdrawn to measure the insulin level using a rat insulin ELISA kit.

3.2.10 Paracetamol absorption test

To evaluate effects on gastric emptying, a solution of paracetamol (100 mg/kg) was given orally, and blood was collected from the tail vein at scheduled times of 0, 15, 30, 60, 90, 120 and 180 min. The collected blood was centrifuged to obtain the plasma, 10 μ l of which was mixed with 90 μ l methanol. Then, 50 μ l of the supernatant was collected and dried with a speedvac (Thermo Fisher Scientific, USA) for 12 h. The resulting pellet was dissolved in a mixture of 45 μ l of deionized water at pH 2.5 and 15 μ l of ACN for measurement. The paracetamol concentration was measured with a LC/MS system (6120 series, Agilent Technologies, USA) with a C18 column (5 μ m, 4.6 mm \times 250 mm, Agilent Technology, USA). The mobile phase was composed of deionized water at pH 2.5 and ACN (v/v, 75:25). The flow rate was 2 ml/min and the detection wavelength was 207 nm.

3.2.11 Histology and immunohistochemistry

At the end point of the experiments, the rats were fasted overnight and sacrificed by cardiac puncture under isoflurane anesthesia. After PBS perfusion, pancreas and adipose tissues were extracted immediately. The collected tissue

was then fixed in a formalin solution and embedded in paraffin to prepare a block, which was cut into 4- μm thick slices for staining. To assess the pancreas tissue, β -cells were detected with immunohistochemistry (IHC); the samples were treated with a rabbit anti-rat insulin antibody (1:300) followed by a goat anti-rabbit IgG-HRP antibody (1:100). The whole slide was visualized with a Vector NovaRED Peroxidase (HRP) Substrate kit and scanned with a SCN400 Slide Scanner (Leica Microsystems, Germany). In each scanned image, the insulin-positive area was presented as percent based on the whole pancreas area. To assess the adipose tissue, the slide was stained with haematoxylin and eosin (H&E), which was imaged with an optical microscope (BX53, Olympus, Japan) at a magnification of $\times 200$. To assess the cross-sectional area of adipocyte, >100 cells randomly selected per image using Adiposoft (ImageJ software, National Institute of Health, USA) were measured.

To examine the biocompatibility of the implanted pump, the tissue surrounding the magnetic pump was extracted and divided into four distinct groups according to the locations. Each of the tissue samples was then prepared into slides, which were stained on H&E and Masson's trichrome (MT) to assess the degree of inflammation, based on the number of polymorphonuclear cells, and measure the thickness of the fibrous capsule around the implanted magnetic pump, respectively. The tissue slide was imaged with an optical microscope at a magnification of $\times 200$, and analyzed by a professional pathologist.

3.2.12 Statistical analysis

Data are presented as means \pm standard error of the mean, and differences between groups were determined by one-way analysis of variance (ANOVA) followed by the post hoc Tukey's test for multiple comparisons. Effects of

OGTT and paracetamol absorption were assessed by repeated-measures ANOVA. Statistical analysis was performed with GraphPad Prism 7 (GraphPad Software, USA). Differences were considered to be statistically significant when $P < 0.05$.

3.3 Results

3.3.1 Pump design and working principles

The overall design and primary working principle of the magnetic pump for exenatide delivery herein was based on that of the prototype pump depicted in a previous work (29). The pump was composed mainly of an actuator and reservoir, which were sealed with the top and bottom covers. The actuator consisted of a plunger and barrel, each of which was equipped with the magnets for actuation. Thus, when the magnet from the outside body was applied, the plunger moved to infuse a drug solution in the reservoir towards the outside of the pump. However, considering the applicability in exenatide delivery, the magnetic pump was extensively upgraded, as described below.

To avoid an unwanted, accidental actuation, the plunger and barrel were each embedded with multiple magnets of patterned polarity, like a key and key hole (Fig. 3.4). The patterns of the magnets in the plunger (M_P) possessed polarity opposite to the magnets in the barrel (M_B) and thus, the plunger was attracted to the barrel to prevent movement. Only when the magnets with the same pattern and opposite polarity approached and overcame the attraction forces between the M_P and M_B , the plunger was able to move for actuation. For such application of the magnetic force from outside the body, a pen-type external device was prepared, which was also embedded with multiple magnets in a

pattern (M_E). The end of the external device with the M_E was designed to be freely rotatable to allow for easy alignment of the M_E and M_P regardless of the orientation of the external device held by the users.

The reservoir was composed of a drug container and fluid conduit that were connected in series (Fig. 3.4). The drug container was made of a flexible biomaterial, polyurethane, to avoid negative pressure build-up due to drug consumption after multiple actuations. The fluid conduit was assembled with an inlet valve, silicone tube and outlet valve in series. The silicone tube served as an intermediate container of a drug solution during actuation, where those two valves were purposed to prevent any possible backflow of the drug solution already in the silicone tube and bodily fluid outside the pump, respectively. Unlike the previous pump, the drug solution in the reservoir could be completely isolated from the actuator, and thus, it was mostly in contact with the constituent material of the drug container only, hence better maintaining the drug stability. The drug container was also equipped with a refill port for replenishment via needle injections even after implantation considering semi-permanent use of the pump. The refill port was shaped to be slightly protruded for ease of localization when the pump was still inside the body (Fig. 3.5). Fig. 3.6 shows an optical image of the magnetic pump and external device.

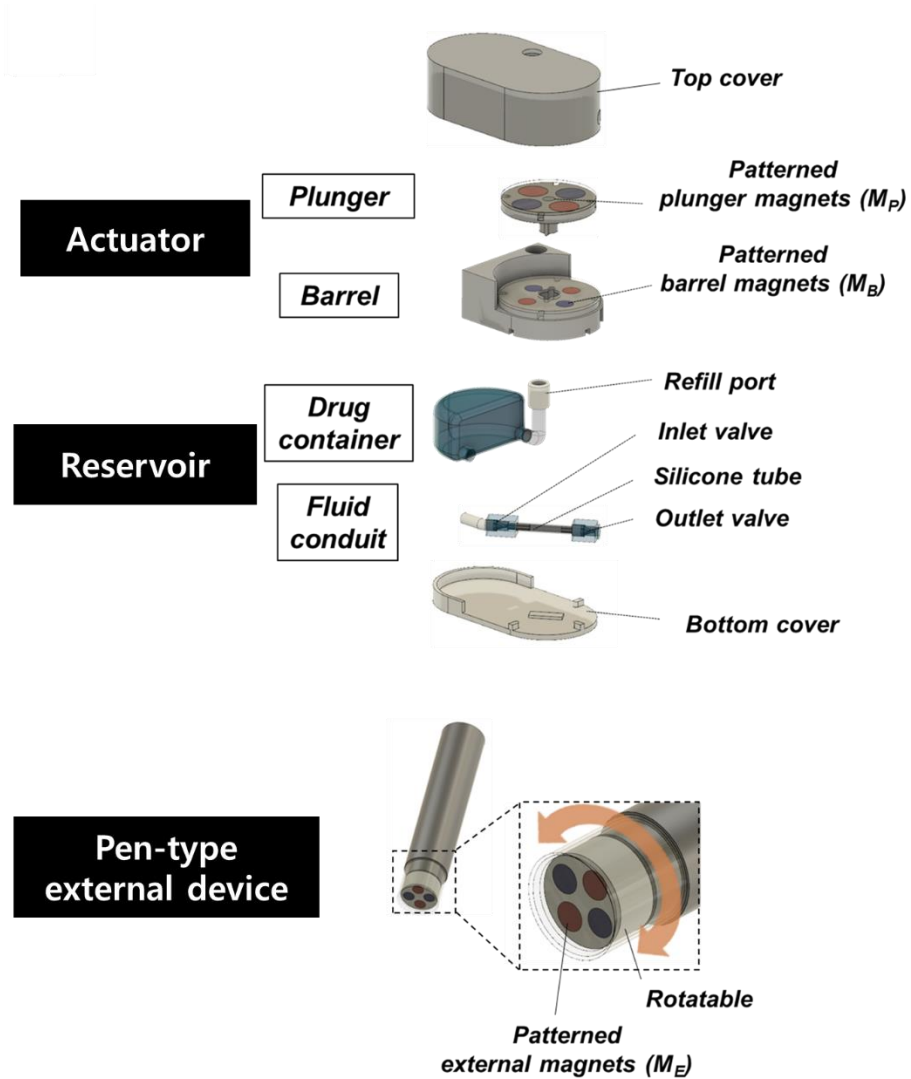


Figure 3.4 3D schematic of the pump.

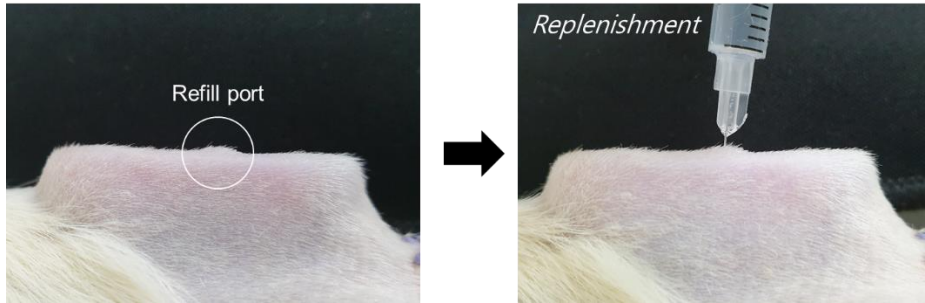
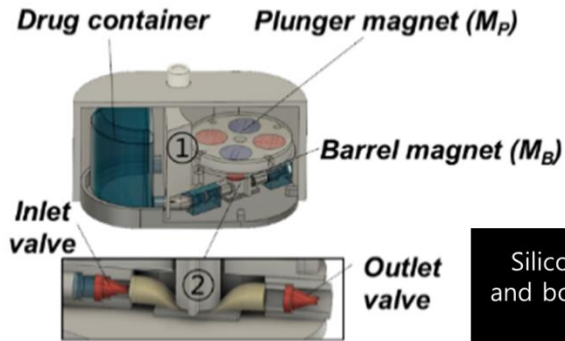


Figure 3.5 Refill port after implantation. The refill port is slightly protruded in the skin, which can be easily visualized during the replenishment procedure.

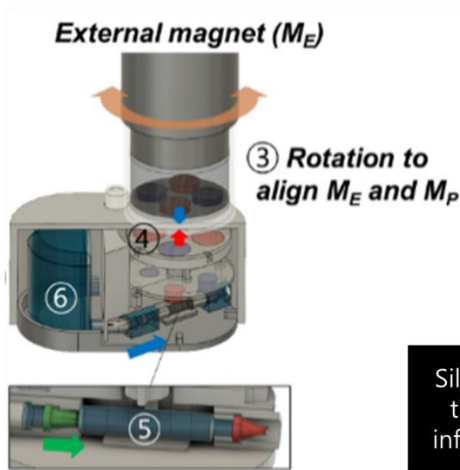


Figure 3.6 Optical image of the pump and external device with patterned magnets. The scale bar is 1 cm.

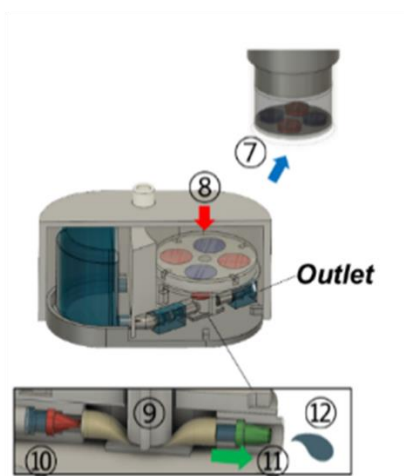
Fig. 3.7 shows the actuation principle of the magnetic pump. During no actuation, the patterned M_P and M_B with an opposite polarity fixes the plunger to tightly press the silicone tube (Fig. 3.7 ①), thereby a minimal amount of residual drug solution and no drug leakage as both inlet and outlet valves are closed (Fig. 3.7 ②). When the external device is applied to the magnetic pump from the outside body, the end of the external device rotates to align M_E with M_P (Fig. 3.7 ③). As their attraction force is designed to be stronger than that between M_P and M_B , the plunger is lifted (Fig. 3.7 ④) to expand the silicone tube and create a negative pressure, which opens the inlet valve while the outlet valve is still closed, allowing for infiltration of the drug solution in the container into the silicone tube (Fig. 3.7 ⑤). During this process, the drug container shrinks; however, due to flexibility, a negative pressure build-up can be minimized (Fig. 3.7 ⑥). When the external device is removed (Fig. 3.7 ⑦), the plunger moves downward due to the attraction between M_P and M_B (Fig. 3.7 ⑧), which compresses the silicone tube (Fig. 3.7 ⑨). An increase in pressure inside the silicone tube closes the inlet valve (Fig. 3.7 ⑩) and opens the outlet valve (Fig. 3.7 ⑪) to infuse the drug solution through the outlet (Fig. 3.7 ⑫).



Silicone tube is compressed, and both inlet and outlet valves are closed



Silicone tube expands to open the inlet valve and allow for infiltration of the drug solution



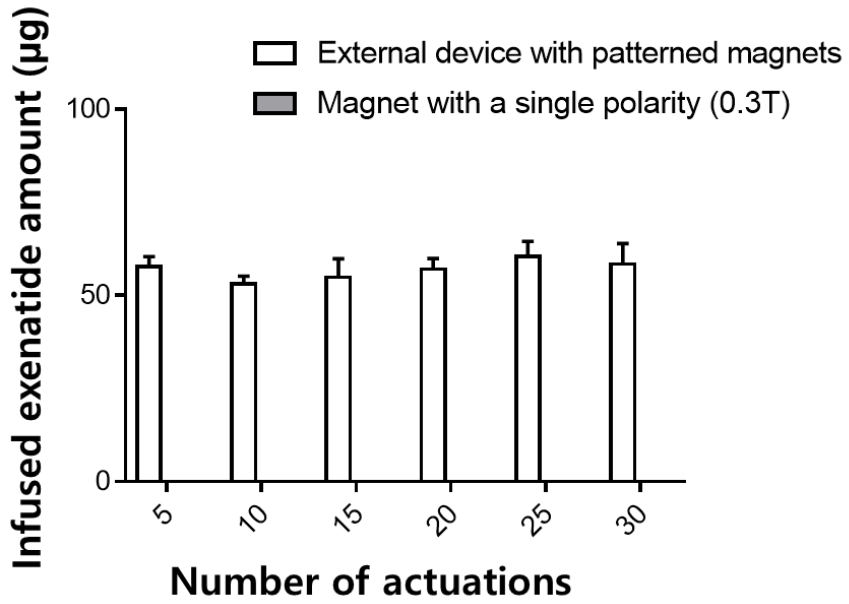
Silicone tube is compressed to open the outlet valve and infuse the drug solution

Figure 3.7 Actuation principle of the pump.

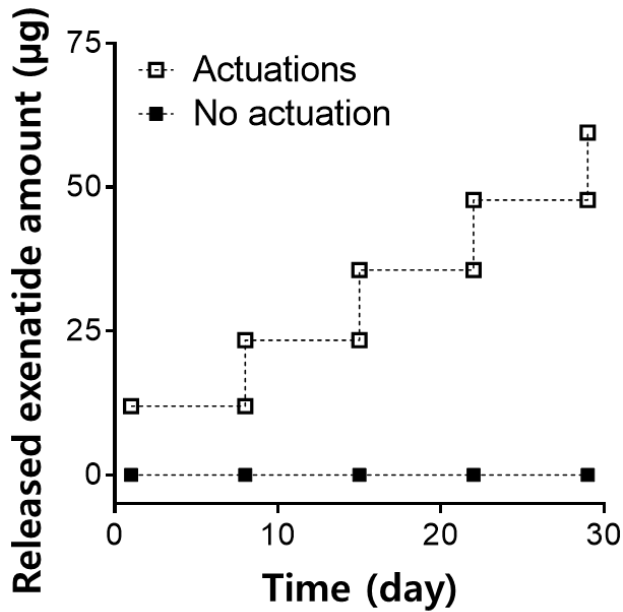
3.3.2 In vitro performance test

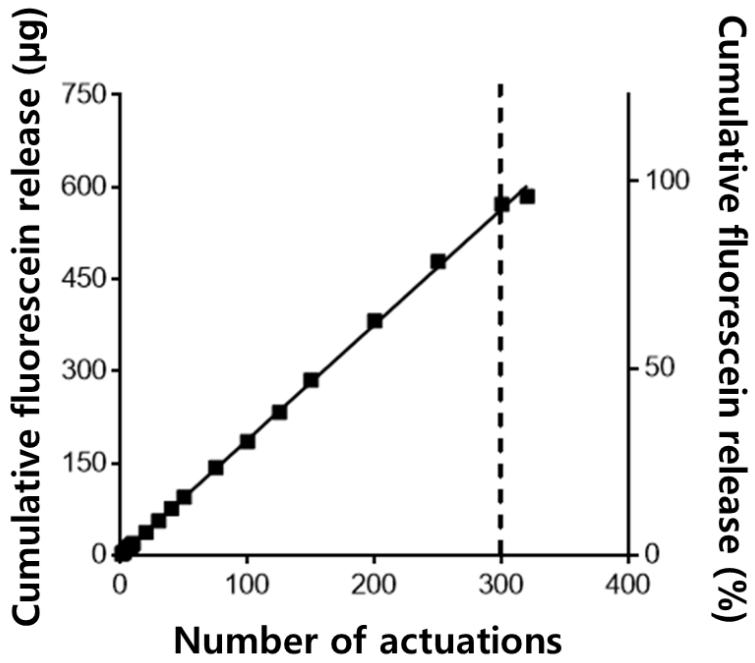
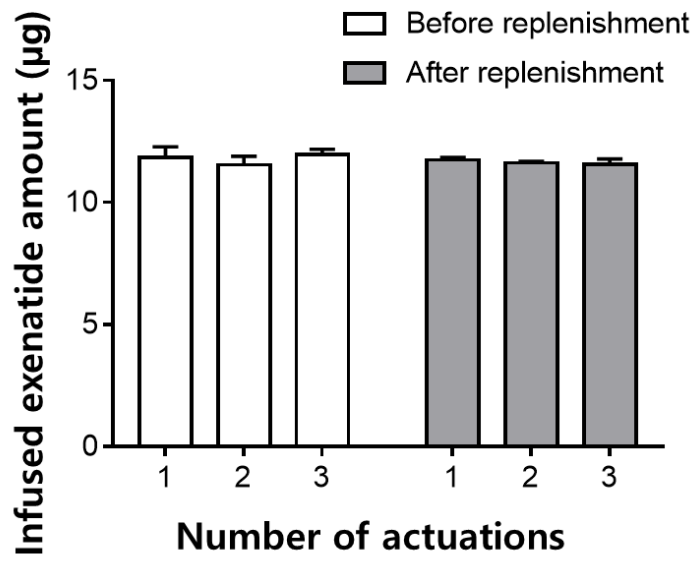
To test the performance, the magnetic pump herein was first tested under in vitro environments. For this, the pump was fully immersed in pH 7.4 PBS and the external device was applied on top of the pump at a gap of 1 mm to simulate the presence of skin after pump implantation (62). As shown in Fig. 3.8A, the drug was infused reproducibly at a bolus exenatide dose of $11.4 \pm 0.3 \mu\text{g}$ per actuation (equivalent to $1.82 \pm 0.05 \mu\text{l}$ of liquid infusion per actuation) using the silicone tube as an intermediate container. Meanwhile, the pump did not release any exenatide when a strong magnet with a single polarity (i.e., a magnet without patterns) was applied (Fig. 3.8A). While the pump was immersed in PBS for a long time over 28 days, the dose per actuation was still reproducible and the drug leak was not observed during no actuation periods due to the presence of the check valves (Fig. 3.8B). Immediately after the removal of the external device, the compression force over the silicone tube was governed mainly by the attraction force between M_P and M_B and thus, the infusion volume could be reproducible, leading to a reproducible drug dose per actuation. With the use of a flexible drug container, the magnetic pump exhibited a reproducible infusion per actuation with up to 300 consecutive actuations until consuming about 94% of the total volume of the solution in the container (Fig. 3.8C). The reproducible infusion profile per actuation was not influenced by the replenishment procedure employed in this work (Fig. 3.8D). Exenatide in the pump was stable without apparent denaturation when stored in the device at 37°C for 4 weeks (Fig. 3.8E and F).

A



B



C**D**

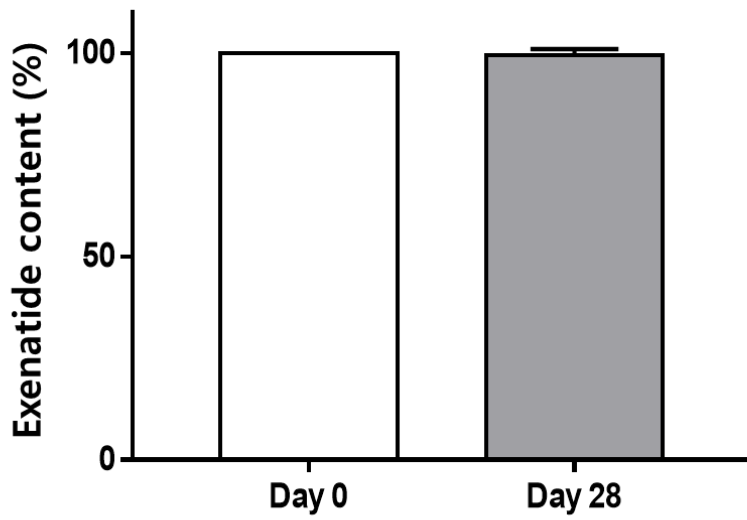
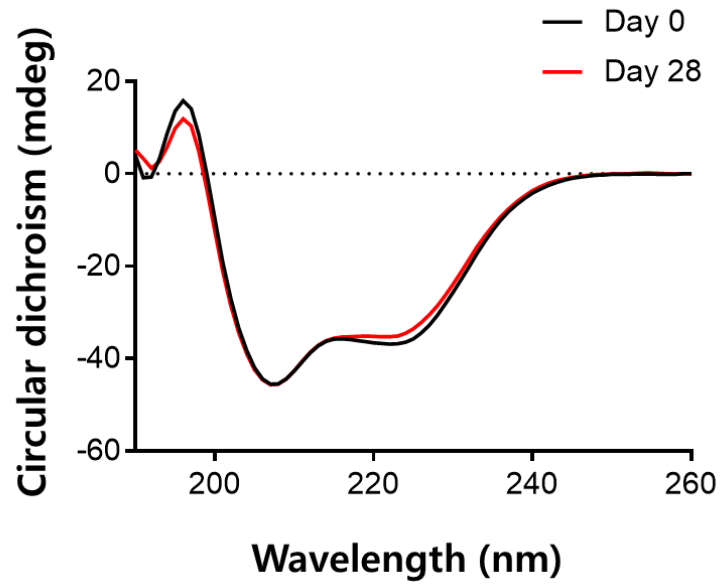
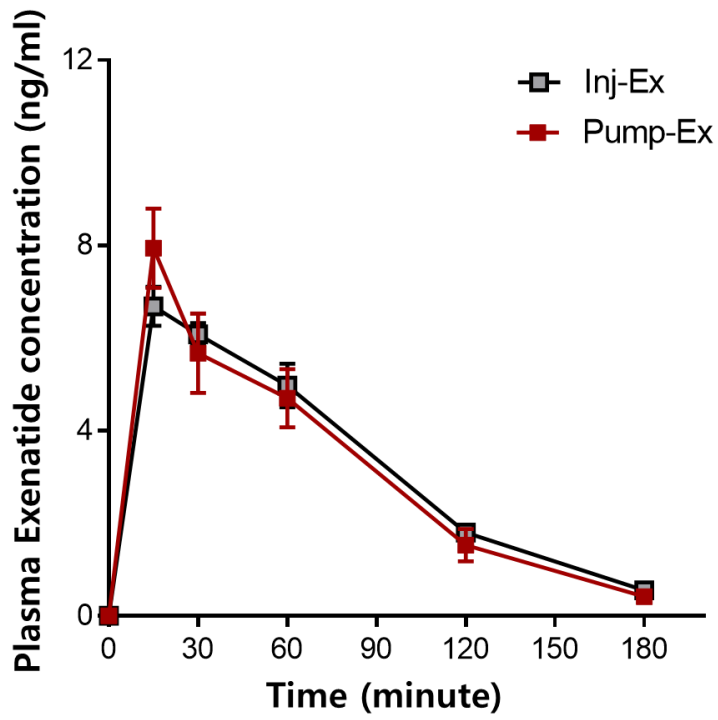
F**F**

Figure 3.8 In vitro performance test of the magnetic pump. (A) The magnetic pump loaded with exenatide was actuated three times before and after a replenishment procedure ($n = 3$). The infused dose per actuation did not vary significantly, indicating that the replenishment procedure did not affect the performance of the magnetic pump. (B) The pump was either actuated at predetermined times of 1, 8, 15, 22 and 29 days or left unactuated while being fully immersed in PBS ($n = 5$). Given the LOQ (limit of quantification of the measurement, $5 \mu\text{g/ml}$) in this work, the leak, if any, would be $< 0.625 \mu\text{g}$ per day. (C) Accelerated depletion test. The pump was loaded with a solution of a model compound, fluorescein (1 mg/ml) instead and actuated consecutively up to 320 times until depletion. The magnetic pump exhibited a reproducible infusion per actuation ($2.02 \pm 0.05 \mu\text{g}$ fluorescein per actuation equivalent to $2.02 \pm 0.05 \mu\text{l}$ of liquid infusion per actuation) with up to 300 consecutive actuations. (D) Thirty consecutive actuations were applied with external device with patterned magnets or a strong magnet with a single polarity (0.3 T). The amount of drug newly released from the pump was measured after every five consecutive actuations ($n = 3$). Stability evaluation of exenatide assessed with (E) HPLC ($n = 3$) and (F) CD spectroscopy after storing in the pump at 37°C for 28 days. Error bars are \pm standard error of the mean.

3.3.3 In vivo pharmacokinetic tests

To evaluate the in vivo performance, the pharmacokinetic profiles of exenatide were compared between the two different animal groups: Pump-Ex and Inj-Ex group. For both groups, the same dose of exenatide was administered. As shown in Fig. 3.9, the pharmacokinetic profiles of exenatide from the Pump-Ex and Inj-Ex groups were superimposable with a similar maximum plasma concentration (C_{max}) of 7.94 ± 0.74 ng/ml and 6.69 ± 0.37 ng/ml, respectively. The time taken to reach the C_{max} (T_{max}) was 15 min in both groups. The areas under the drug concentration curve (AUC) were nearly identical as 20.3 ± 1.5 and 20.1 ± 0.9 ng/ml min for the Pump-Ex and Inj-Ex groups, respectively. The pharmacokinetic profile shown above remained unaltered even after a replenishment procedure with the implanted magnetic pump (Fig. 3.10).

A



B

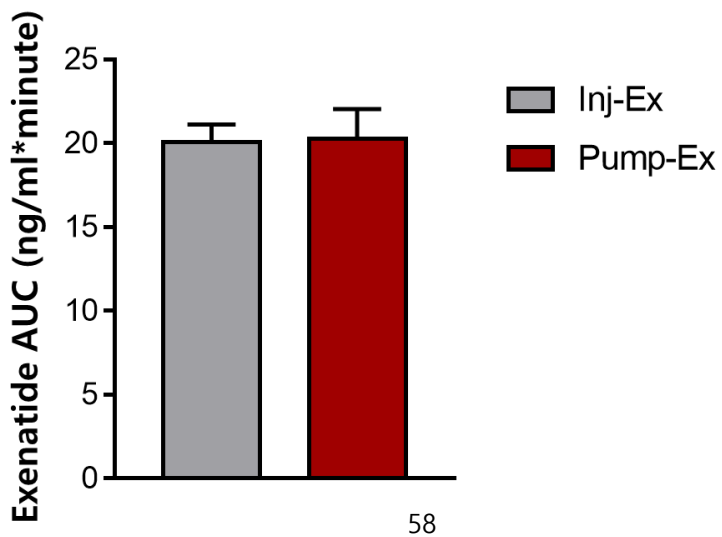
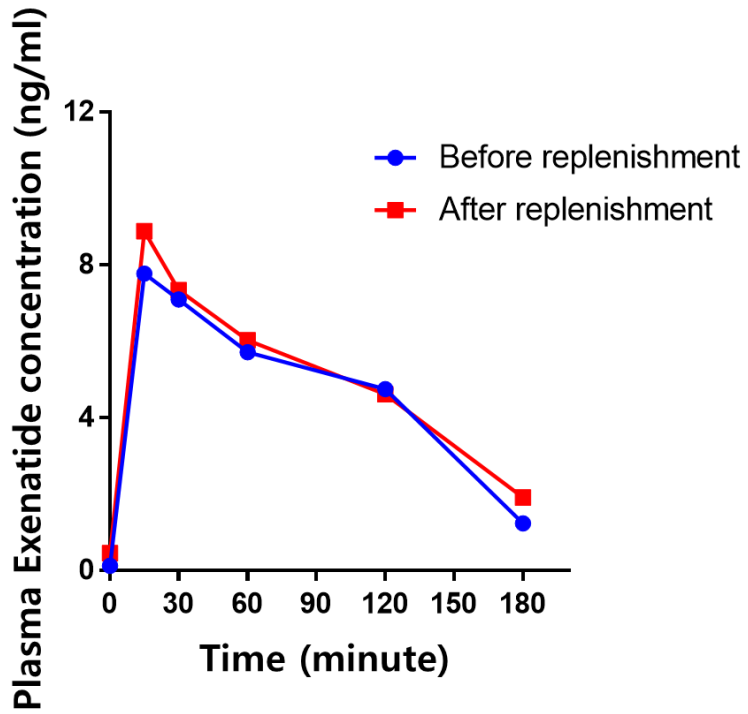


Figure 3.9 In vivo pharmacokinetic profiles of exenatide. (A) The exenatide concentration in blood plasma was measured using an exenatide enzyme immunoassay (EIA) kit (n = 4). (B) AUC was calculated using the trapezoidal rule, which was not statistically significantly different between the Inj-Ex and Pump-Ex groups ($P > 0.05$; Student's t-test). Error bars are \pm standard error of the mean.

A



B

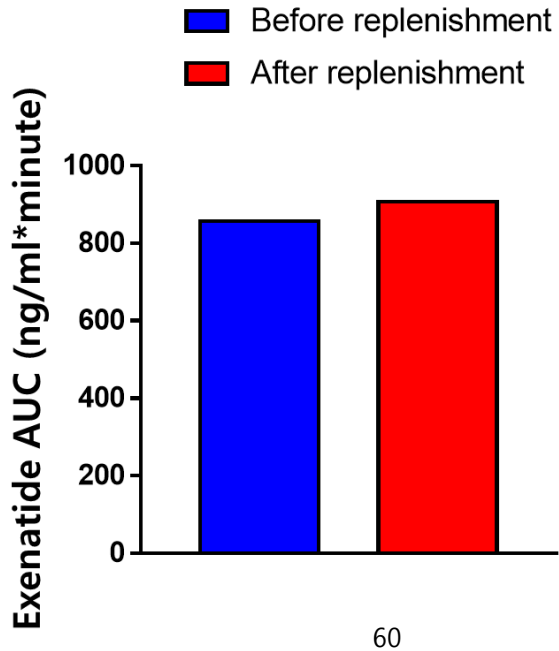


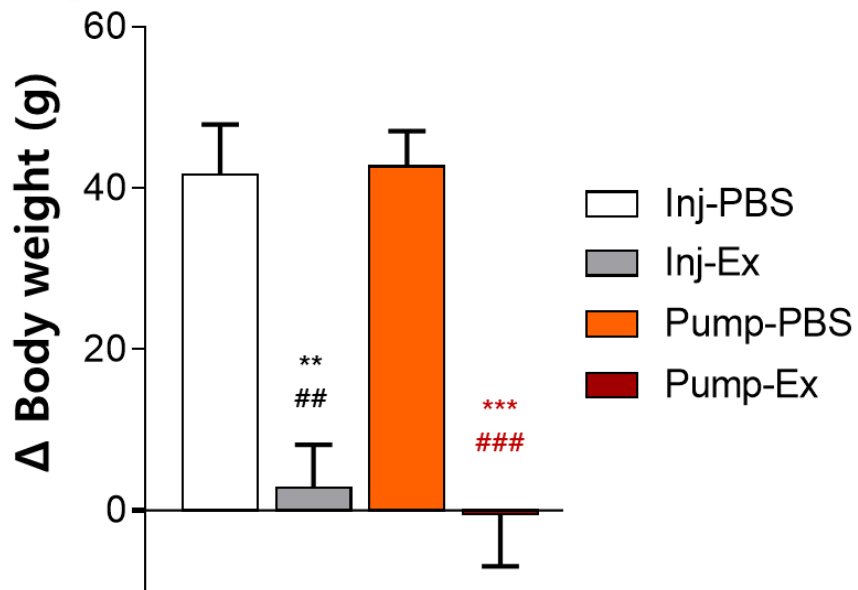
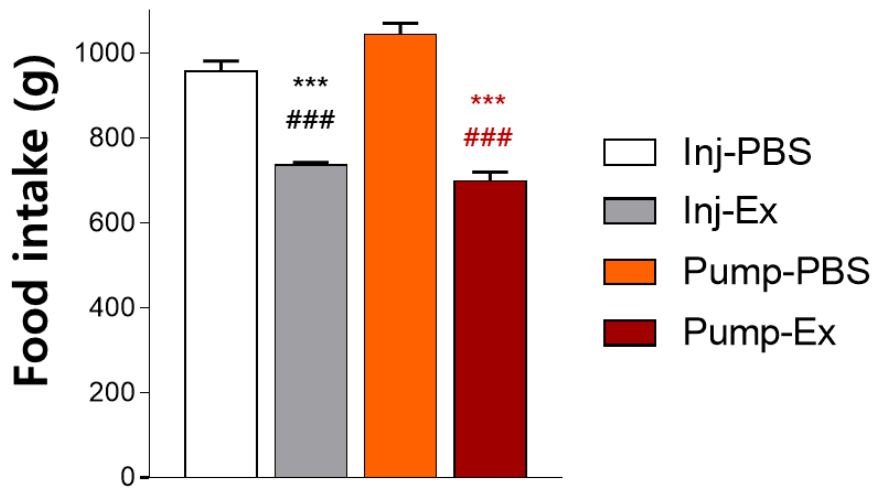
Figure 3.10 Reproducibility assessment of the magnetic pump after a replenishment in vivo. The magnetic pump loaded with exenatide was implanted in Wistar rats ($n = 1$) and actuated before and after a replenishment procedure. A replenishment procedure was performed when the magnetic pump was implanted in rats. After each actuation, the blood was withdrawn at scheduled times and the plasma concentration of exenatide was measured, as depicted in the Materials and Methods Section. The pharmacokinetic profiles of exenatide in blood plasma did not vary significantly, indicating that the replenishment procedure herein still did not affect the in vivo performance of the magnetic pump.

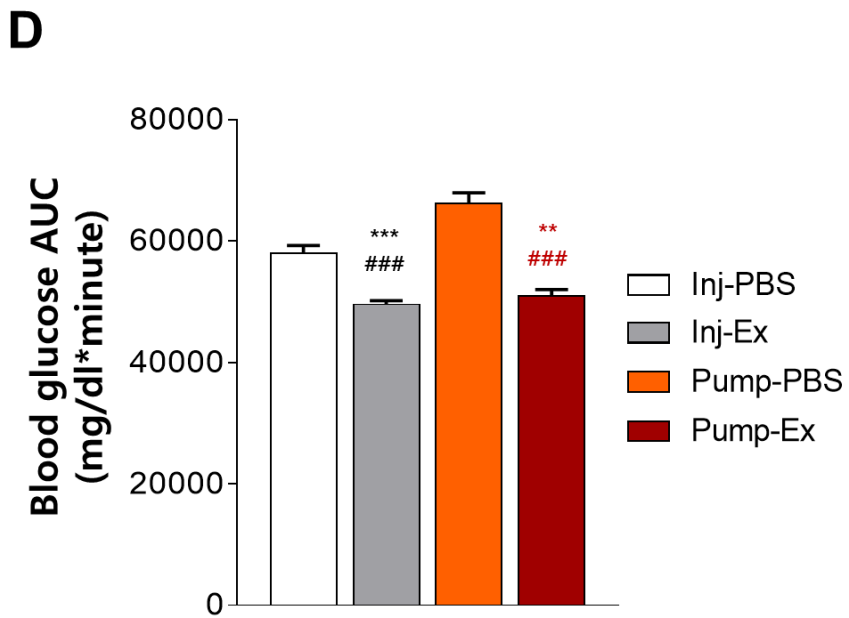
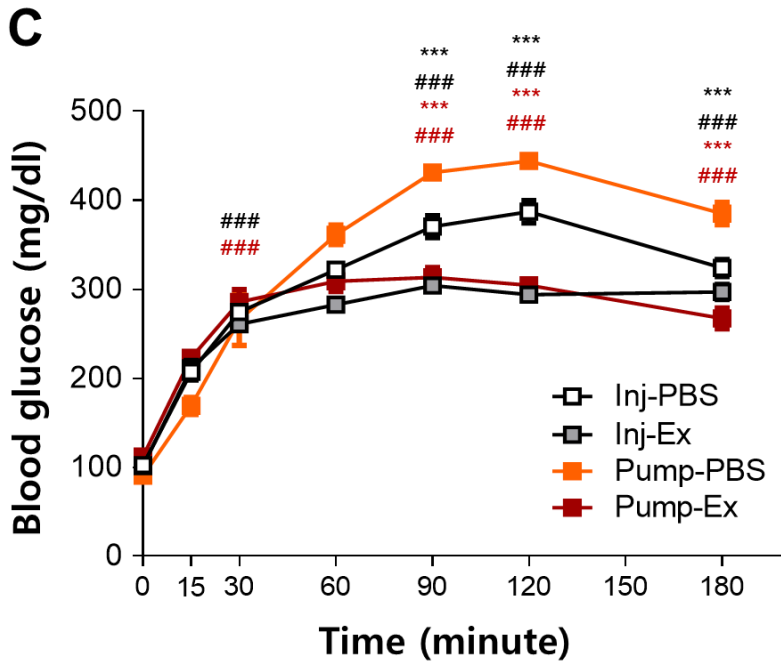
3.3.4 In vivo pharmacodynamic tests

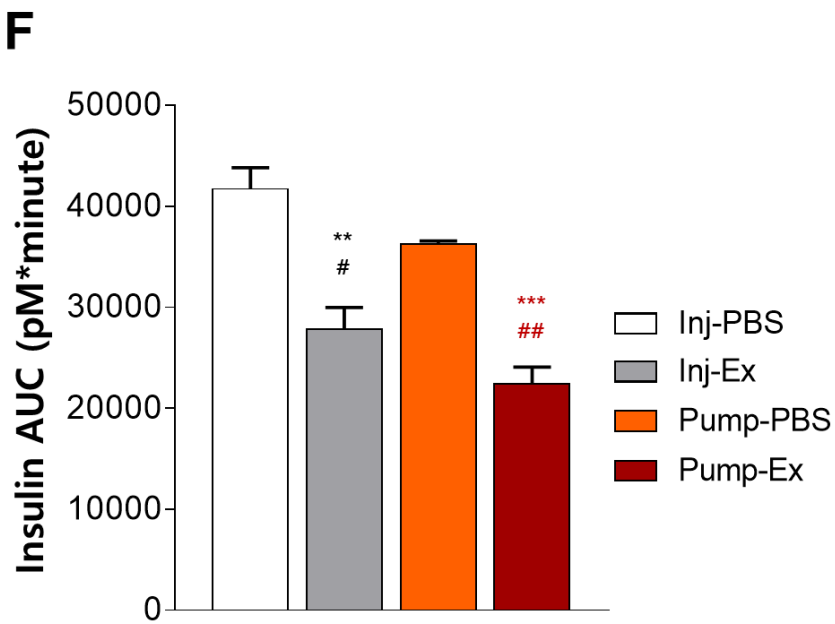
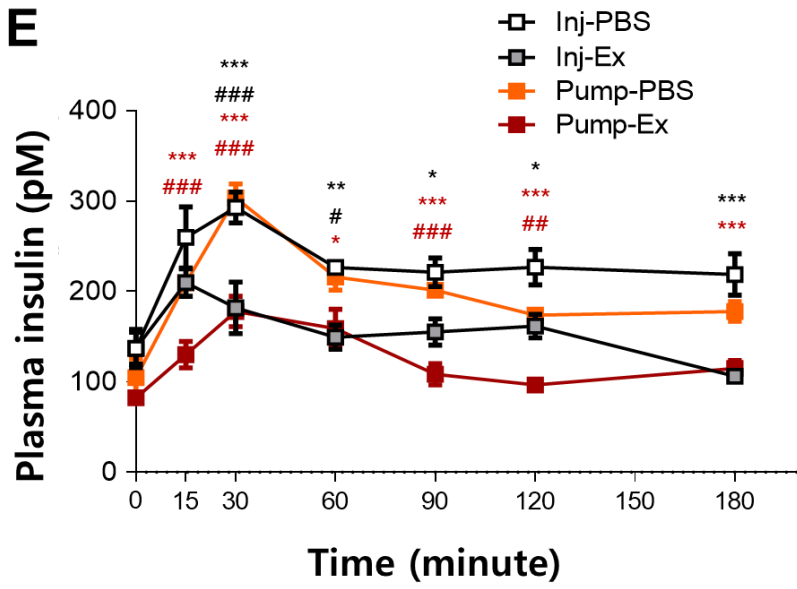
To evaluate the in vivo pharmacodynamics of exenatide, two more animal groups were added for a total of four different animal groups: (i) Inj-PBS, (ii) Pump-PBS, (iii) Inj-Ex, and (iv) Pump-Ex groups. For all groups, the same volume of exenatide solution or PBS without exenatide was administered twice per day for 7 weeks, respectively.

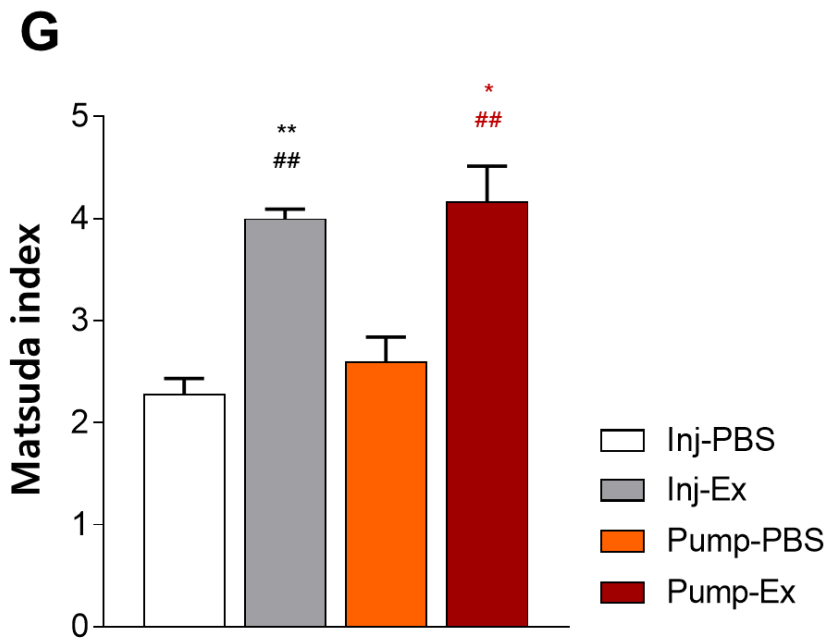
For the parameters of pharmacodynamics, the profiles of body weight and food intake were measured (63, 64). As shown in Fig. 3.11A, the GK rats treated with exenatide (both the Inj-Ex and Pump-Ex groups) exhibited a significantly lower body weight gain than those treated with PBS only (both the Inj-PBS and Pump-PBS groups) ($P < 0.05$). In accordance with this, the total food intakes in both exenatide groups were significantly lower than those of both PBS groups ($P < 0.05$; Fig. 3.11B). During the OGTT performed after 6 weeks of treatment, there were no significant differences in pharmacodynamic parameters related to postprandial glucose metabolism between the Inj-Ex and Pump-Ex groups. The blood glucose levels after a glucose load were lower with both exenatide groups compared with both PBS counterparts (Fig. 3.11C). The area under the plasma glucose concentration-time curve (AUC_{glucose}) of both exenatide groups was significantly lower than those of the PBS-treated groups (Fig. 3.11D). The plasma insulin levels during the OGTT in both exenatide groups were lower than those with both PBS-treated groups (Fig. 3.11E). The AUC_{insulin} was significantly lower in both exenatide-treated groups than those in the respective PBS-treated groups (Fig. 3.11F). Insulin sensitivity during the OGTT, which was measured by the Matsuda Index (65), was significantly higher in both exenatide groups compared with both PBS groups (Fig. 3.11G).

To examine the gastric emptying rate, the paracetamol absorption rate after 6 weeks of treatment was measured (58). The plasma paracetamol levels were lower in the both exenatide groups than both PBS groups (Fig. 3.11H), and the corresponding $AUC_{\text{paracetamol}}$ was significantly lower in the exenatide groups than in the respective PBS groups ($P < 0.05$, Fig. 3.11I). This lower systemic absorption of orally-administered paracetamol suggested more delayed gastric emptying by exenatide administrations, which could explain a lower food intake and body weight gain (Fig. 3.11A and B), as well as improved glucose tolerance (Fig. 3.11C-G). Most importantly, there was no significant difference in the above-mentioned pharmacodynamic parameters between the Inj-Ex and Pump-Ex groups, suggesting that the efficacy of the exenatide delivered with the pump herein was nearly identical to that administered via SC injections.

A**B**







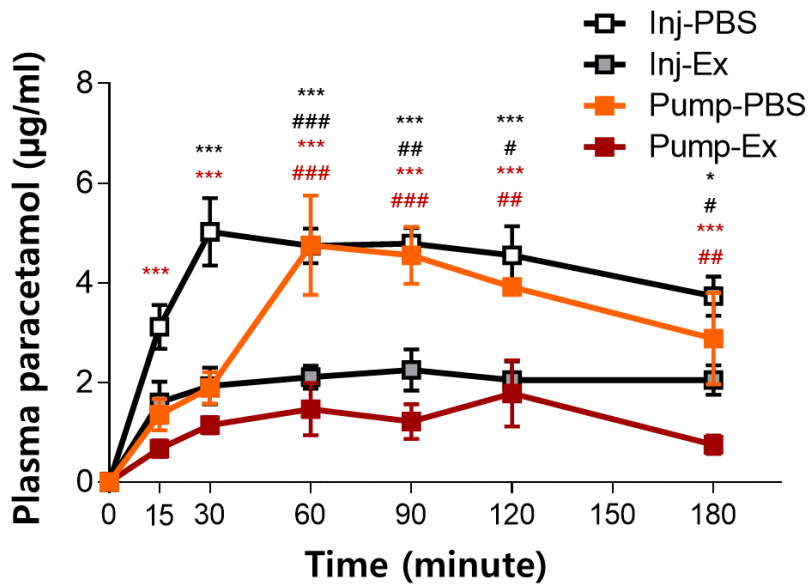
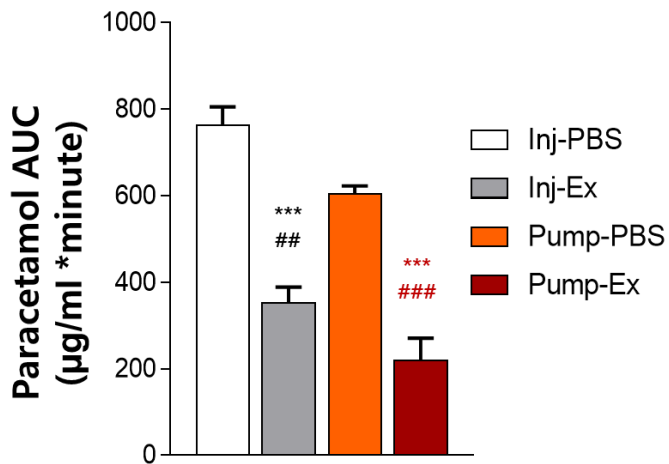
H**I**

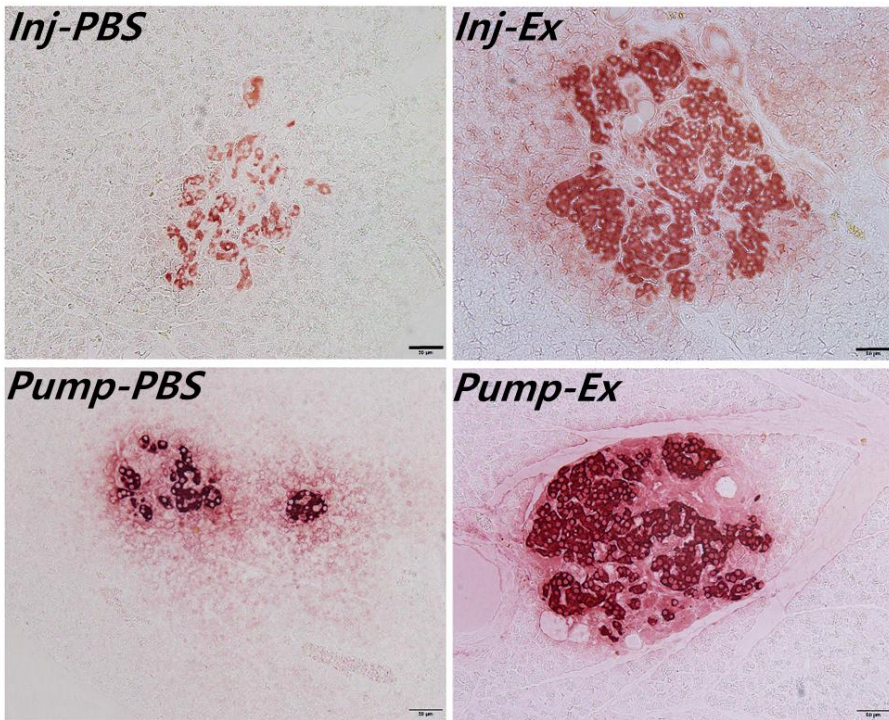
Figure 3.11 Pharmacodynamic profiles of exenatide. Profiles of (A) body weight change and (B) total food intake after the 7-week treatment of GK rats. Data are shown as means \pm standard error ($n \geq 4$). Profiles of (C), (D) blood glucose concentrations and (E), (F) plasma insulin concentrations, where the AUC of each parameter was calculated using the trapezoidal rule. (G) The Matsuda index was obtained to estimate insulin sensitivity. Data are shown as means \pm standard error ($n \geq 4$). Profiles of (H) plasma paracetamol excursions and (I) AUC, which was calculated by the trapezoidal rule. Data are shown as means \pm standard error of the mean ($n \geq 4$). Black * indicates Inj-Ex versus Inj-PBS and Red * indicates Pump-Ex versus Inj-PBS, where *P < 0.05, **P < 0.01 and ***P < 0.001. Black # indicates Inj-Ex versus Pump-PBS and Red # indicates Pump-Ex versus Pump-PBS, where #P < 0.05, ##P < 0.01 and ###P < 0.001.

3.3.5 Effects on the pancreatic islets and adipose tissues

GK rats are an animal model characterized by pancreatic β -cell loss and islet fibrosis leading to their bizarre-looking shape (66), which was clearly observed with the PBS-treated groups (Fig. 3.12A). Alternatively, the pancreatic islet structure was relatively well preserved in both exenatide-treated GK rats. The β -cell areas measured by insulin staining were significantly greater in both exenatide-treated groups than in the PBS-treated groups (Fig. 3.12B).

Although the GK rat is a non-obese diabetic animal model, the H&E-stained tissues revealed that the size of adipocytes in the epididymal fat pad was smaller in both the exenatide-treated groups than in the PBS-treated groups (Fig. 3.13). In addition, inflammation appeared to decrease in visceral adipose tissues, which was assessed by the number of crown-like structures, in the both exenatide-treated groups compared to the corresponding PBS-treated groups (Fig. 3.14). However, in the subcutaneous and brown adipose tissues, there was no apparent morphological difference among the tested animal groups (Fig. 3.15). These results suggest a similar effect of exenatide on the protection of pancreatic β -cells, as well as on the reduction of visceral fat, between the Inj-Ex and Pump-Ex groups.

A



B

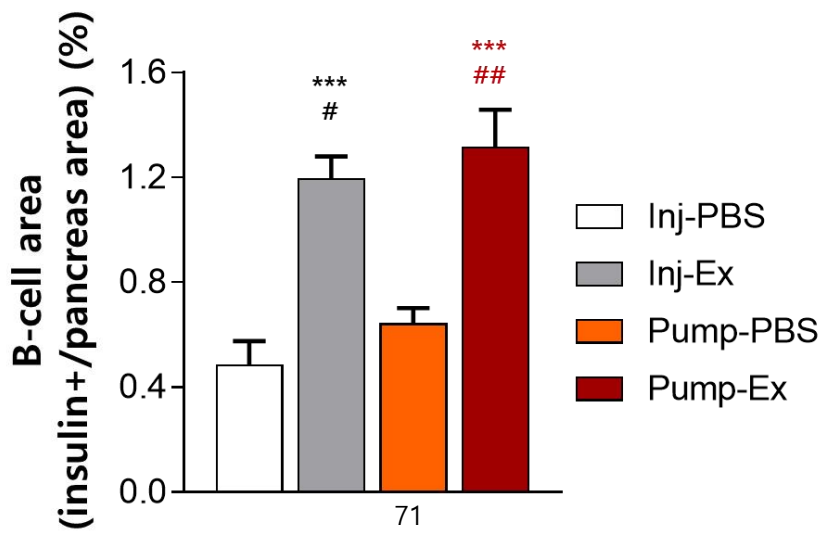
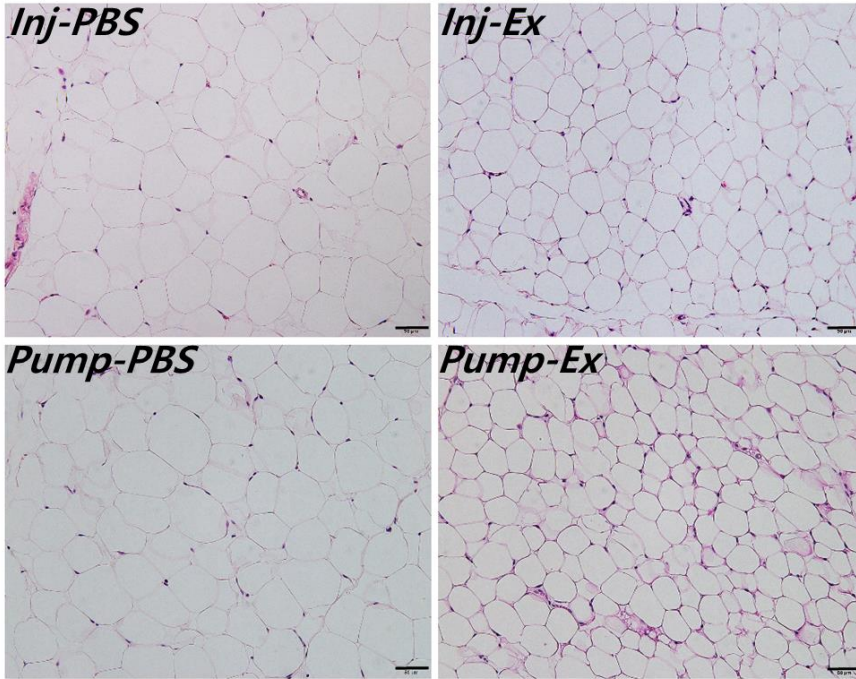


Figure 3.12 Profiles of pancreatic islet structure. (A) Representative IHC-stained images, showing brown colors as insulin positive in the pancreas tissue sections. The scale bars are 50 μm . (B) Histomorphometric quantification of the β -cell area was calibrated as percent based on the whole area of pancreatic tissues ($n \geq 4$). At least three images randomly selected per rat were examined for statistics. Data are shown as means \pm standard error. Black * indicates Inj-Ex versus Inj-PBS and Red * indicates Pump-Ex versus Inj-PBS, where ***P < 0.001. Black # indicates Inj-Ex versus Pump-PBS and Red # indicates Pump-Ex versus Pump-PBS, where #P < 0.05, ##P < 0.01 and ###P < 0.001.

A



B

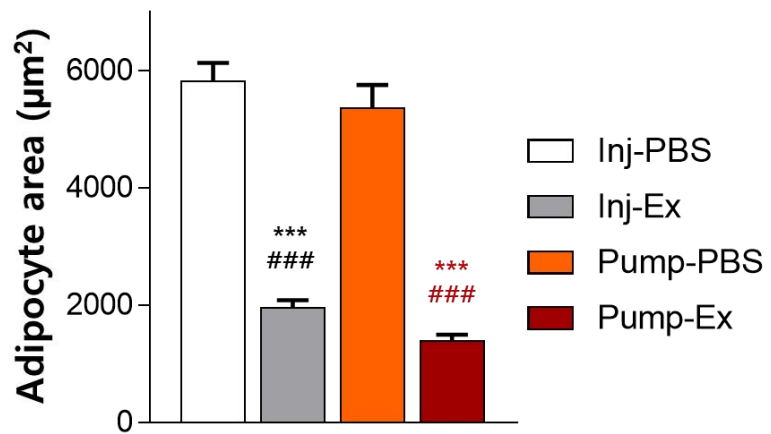


Figure 3.13 Profiles of adipocytes in the epididymal fat pad in GK rats. (A) Representative H&E-stained images of the epididymal adipose tissue sections. The scale bars are 50 μm . (B) Mean cross-sectional areas of adipocytes ($n \geq 4$). At least four images per rat were analyzed for statistics. Data are shown as means \pm standard error. Black * indicates Inj-Ex versus Inj-PBS and Red * indicates Pump-Ex versus Inj-PBS, where ***P < 0.001. Black # indicates Inj-Ex versus Pump-PBS and Red # indicates Pump-Ex versus Pump-PBS, where #P < 0.05, ##P < 0.01 and ###P < 0.001.

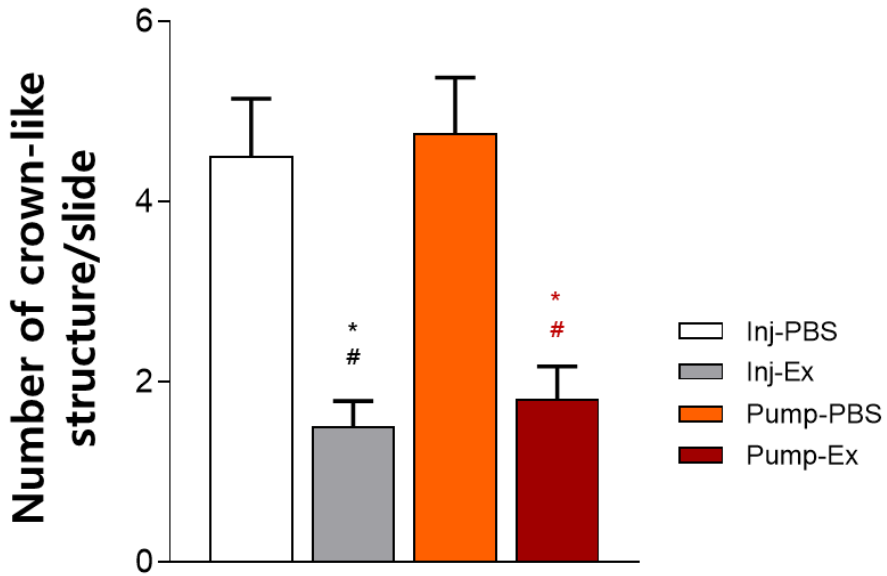


Figure 3.14 Number of crown-like structures in epididymal adipose tissues.

Data are shown as means \pm standard error of the mean ($n \geq 4$). At least four slides per rat were randomly selected and assessed for statistics. * statistically significantly different from the Inj-PBS ($P < 0.05$). # statistically significantly different from the Pump-PBS ($P < 0.05$).

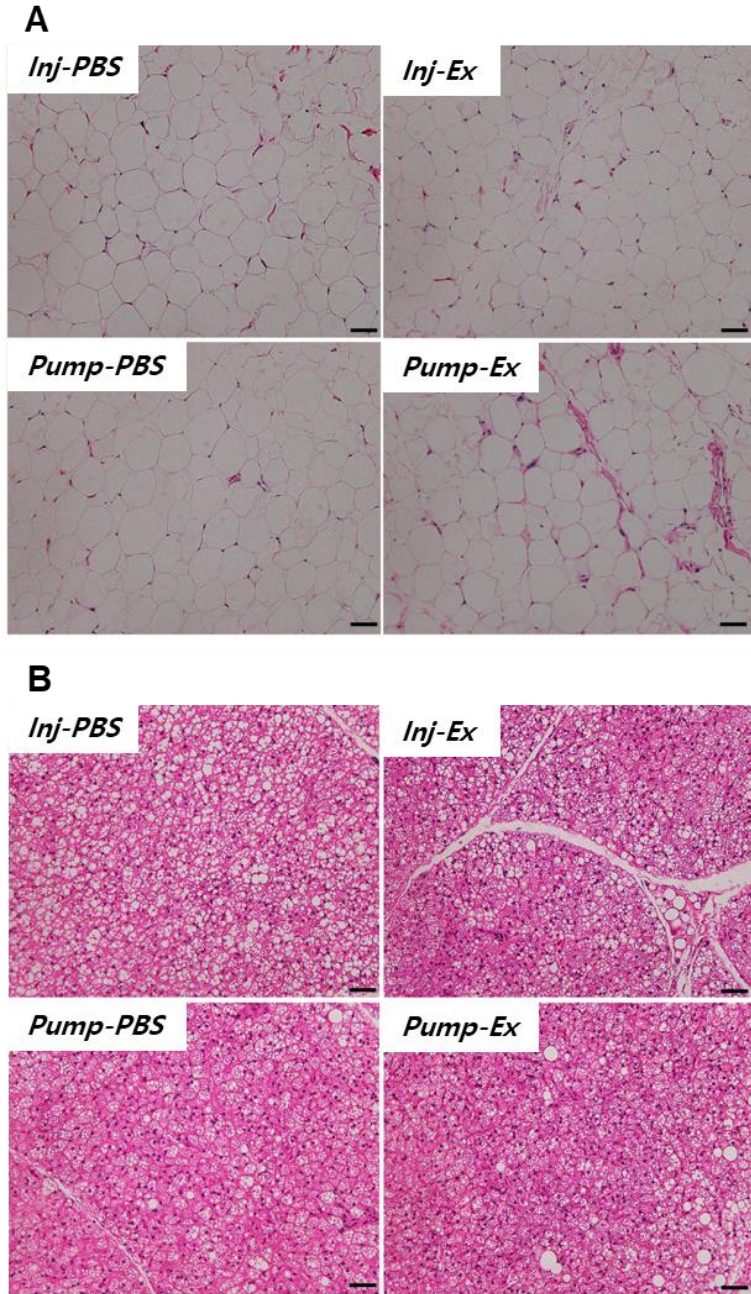
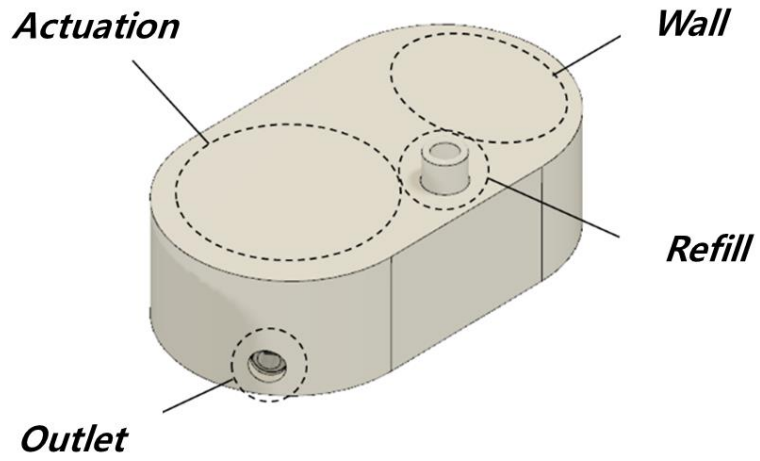


Figure 3.15 Representative H&E-stained images of (A) subcutaneous and (B) brown adipose tissues. The images were obtained at $\times 200$ magnification. The scale bars are 50 μm .

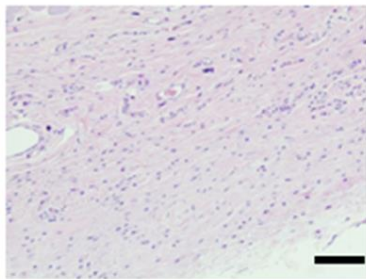
3.3.6 Biocompatibility assessment

To assess the biocompatibility of the magnetic pump, tissues from the four different locations around the magnetic pump were analyzed. The tissues were adjacent to 1) the outlet, 2) the area above the magnet for actuation (i.e., the actuation), 3) an area not used for actuation (i.e., the wall) and 4) the refill port (i.e., the refill) (Fig. 3.16A). The biopsied tissues were treated on H&E and Masson's trichrome (MT) staining, respectively. As shown in Fig. 3.16B, regardless of the tissue locations, mild inflammation with an insignificant number of polymorphonuclear cells was observed around the implanted pump. The MT-stained tissues exhibited the formation of a fibrotic capsule around the implanted pump, the thickness of which was measured as $115.5 \pm 30.3 \mu\text{m}$ (Fig. 3.16C). Such capsule formation was also observed with the implanted devices in other previous studies (22, 29, 67). Fibrotic tissues did not appear to occlude the outlet valve as the outlet valve was seamlessly closed during no actuation periods, and was opened for a very short time (< 1 second) only at the moment the plunger compressed the silicone tube to build up a positive pressure (29). The capsule tissues showed minimal proliferation of benign-looking fibroblasts and rich collagenous stroma, as well as some lymphoplasmacytic, histiocytic and eosinophilic infiltration. The outlet was not blocked when observed at the end point of the experiments (i.e., 52 days after implantation). Inflammation markers in the blood, such as interleukin (IL)- 1β , IL-6 and tumor necrosis factor (TNF)- α , did not vary or increase significantly with the animals implanted with the pump for 52 days (Table 3.1).

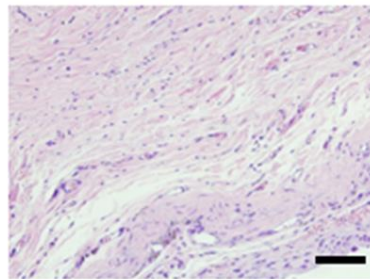
A



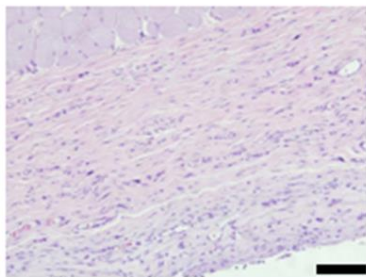
B



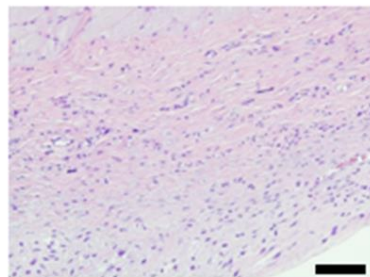
Outlet



Wall



Actuation



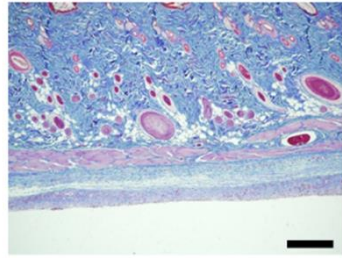
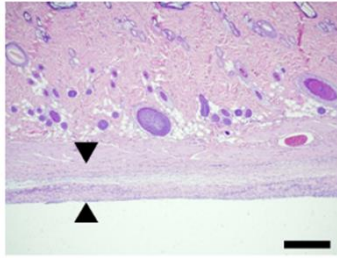
Refill

C

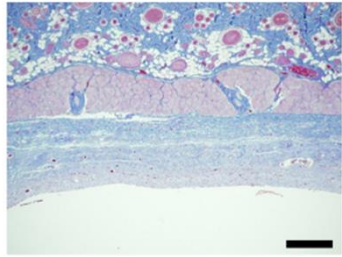
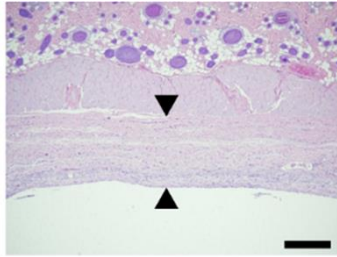
H&E

MT

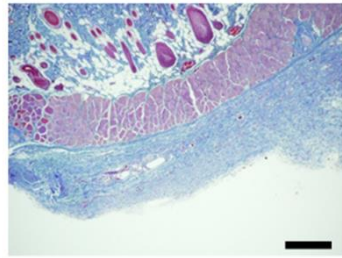
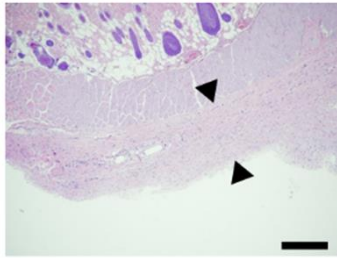
Wall



Actuation



Outlet



Refill

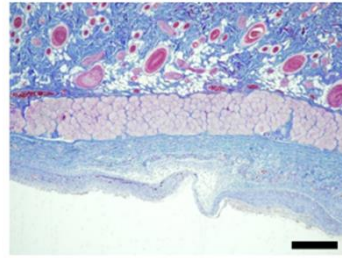
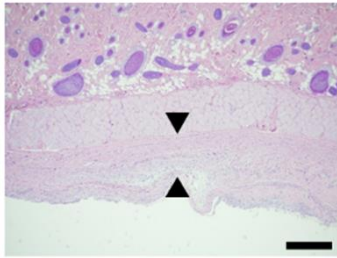


Figure 3.16 Histological images of the tissues around the implanted magnetic pump. (A) Tissue locations around the magnetic pump. (B) H&E-stained tissue images for evaluation of polymorphonuclear cells. (C) H&E- and MT-stained tissue images for evaluation of fibrotic capsule formation, where the arrows indicate the capsule thickness. The scale bars are 100 μm .

Table 3.1 Assessment of inflammatory markers in plasma. Inflammatory markers in plasma, such as IL-1b, IL-6 and TNF- α , were measured at 0 and 52 days after implantation of the magnetic pump ($n \geq 4$). For all animals in the Pump-Ex group, no significant elevation of inflammatory markers was observed compared with the control group, that is, the intact animals without pump implantation. Data are shown as means \pm standard error of the mean.

	IL-1β	IL-6	TNF-α
Control	17.8 \pm 1.3	7.6 \pm 0.6	8.2 \pm 0.4
Pump-Ex (Day 0)	20.8 \pm 2.5	7.2 \pm 0.4	9.8 \pm 0.5
Pump-Ex (Day 52)	12.4 \pm 0.3	7.1 \pm 0.4	7.1 \pm 0.9

(unit: pg/ml)

3.4 Discussions

Recent developments of GLP-1 RAs have focused on reducing dosing frequencies to increase patients' adherence to the injection therapy (68). However, these long-acting GLP-1 RAs are not physiologic because they do not recapitulate the postprandial GLP-1 secretion, thus requiring frequent needed injections of a short-acting GLP-1 RA typically before each meal (25). In this regard, the methodology of exploiting on-demand administrations of a short-acting GLP-1 RA with minimized needed injections could be considered advantageous to address unmet clinical needs.

Therefore, to fill the treatment gap, an implantable, battery-less pump was proposed for on-demand and bolus administration of exenatide. As reported with the pump for insulin delivery in the previous work (29), the pump herein with single implantation was also operable without a battery based on magnetic actuation to allow for on-demand and bolus administration of exenatide without needles only when a noninvasive magnet was applied from outside the body (Fig. 3.7). A refill septum was also featured considering a semi-permanent use after implantation.

In addition to these advantages, the pump in this work was extensively improved considering its translational application for exenatide delivery. Regarding safety, the magnets in the pump and external device were patterned with specific polarities to avoid accidental, unwanted exenatide exposure (Fig. 3.8A). To allow for smooth alignment of the magnets between the plunger and external device, the end of the external device with a specific magnet pattern was designed to be easily rotatable. In addition, a flexible fluid conduit was integrated in the pump, two ends of which were assembled with check valves

and connected to the drug container and outlet port, respectively (Fig. 3.4). In this way, the drug container was better isolated from the bodily fluid, hence better protection of exenatide loaded in the pump. Additionally, the fluid conduit contained the same volume of an exenatide solution, which would be pushed for its bolus release during actuation, thereby a reproducible dose of exenatide (Fig. 3.8A and B).

From the perspective of patients' convenience, it was also aimed to minimize the number of refilling procedures and thus, the drug container was made of a flexible material to prevent negative pressure until nearly all exenatide was consumed by multiple actuations (Fig. 3.8C). The findings revealed that the improved pump exhibited a similar *in vivo* pharmacokinetic profile of exenatide compared with the conventional SC injection (Fig. 3.9). The pharmacodynamic effects in GK rats were nearly identical to those with the SC injections (Fig. 3.11, 3.12, 3.13 and 3.14). Notably, the results in this work were comparable to those from many previous reports that tested the effects of exenatide on rodent models of T2D (57, 59, 63, 64, 69). Combined, the upgraded pump in this work could be a viable and minimally-invasive alternative of a current needled-injection therapy of exenatide for T2D.

The stability of exenatide was monitored for 28 days in this study, and therefore the drug was replenished at day 28 after implantation. However, the exenatide was reported to be delivered for longer than a year in ITCA650 osmotic pump *in vivo*. Also, the magnetic pump could deliver 300 times of drug before a drug replenishment. Therefore, in further studies, the extended stability of exenatide could be evaluated to determine the feasibility of less frequent drug replenishments.

To bring the pump closer to clinical applications for exenatide therapy, more considerations may be needed with respect safety and patient convenience. The exterior of the pump may need to be made of a material with a higher mechanical strength, that is, biocompatible metals, such as titanium or stainless steel (70, 71). A stronger package would better prevent possible rupture of exenatide caused by accidental mechanical impact; however, exenatide does not cause a fatal risk even with a significant overdose (72, 73). The human dose of exenatide is known to be 5 or 10 μg twice a day (74), which is different from the dose per actuation with the pump herein (11.4 μg per actuation). However, this could be easily adapted by changing the exenatide concentration in the container as the pump herein basically infuses a reproducible volume of liquid. In addition, with regard to the administration frequencies of exenatide for humans, the volume of the drug container may need to be increased to approximately 1.5 ml considering replenishment once per year. As the volume of the driving unit for magnetic actuation could be maintained without an increase, the total volume of the pump is expected to be 8.7 ml, which is still approximately 13 times smaller than the implantable drug-delivery pumps already in clinical use (75). If more frequent replenishment is allowed, the volume of the pump could be further decreased. The approximate cost for fabrication of the magnetic pump herein was expected to be not very high (c.a., 20 USD per pump when estimated only with the depreciation of the 3D printer and the consumption of relevant materials). This implies that the magnetic pump herein would not be a significant financial burden to the patients. Instead of a manual application, an external device with electronics could be envisioned to be able to operate the implanted pump and confirm the drug release (76). In this way, a mobile app could be designed to control exenatide administrations

and monitor its regimen history for better safety and usability for patients.

GLP-1 is an incretin hormone that potentiates insulin secretion in a glucose-dependent manner (71). The results revealed that the blood glucose levels after a glucose load during the OGTT markedly decreased with exenatide treatment regardless of the administration methods (Fig. 3.11C and D). Interestingly, however, the plasma insulin levels during OGTT was also lower in both exenatide-treated GK rats than in the PBS-treated counterparts (Fig. 3.11E and F). The paradoxical relationship between the glucose and insulin levels in this study is in accordance with a previous study (57). Thus, the results might be explained by decelerated gastric emptying and improved insulin sensitivity, as assessed by paracetamol absorption and Matsuda index, respectively (Fig. 3.11G-I). GLP-1 slows gastric emptying by mechanisms including relaxation of gastric smooth muscle, reduction of antral and duodenal motility, and an increase in gastric pyloric tone, which are likely to be mediated by vagal pathways (77). GLP-1 can also influence insulin sensitivity in several ways (78). GLP-1 decreases hepatic glucose production possibly through suppression of glucagon secretion by pancreatic α -cell and neural pathways. Weight loss induced by GLP-1 RA can contribute to improving peripheral insulin sensitivity. Collectively, these effects with regard to delayed gastric emptying and enhanced insulin sensitivity could explain the reduced postprandial glucose excursion with lower postprandial insulin levels in this study. Importantly, this was often observed with short-acting GLP-1 RA but not with a long-acting GLP-1 RA that showed nearly no effect on gastric emptying due to tachyphylaxis (25).

Chapter 4

Conclusion and perspective

Minimally-invasive diagnosis and drug therapy are surely the future of diabetes mellitus management. It will free patients from repetitive painful procedures and side effects, and thus enhance patients' compliances and therapeutic effects. However, current methodologies for minimally-invasive diagnosis and drug therapy have drawbacks, so are yet to be considered as practical solutions. For this, a strip-type tear glucose sensor was developed as a methodology of minimally-invasive diagnosis, and an implantable magnetic pump as a methodology of minimally-invasive drug therapy.

In chapter 2, a minimally-invasive self-diagnostic tear-glucose device that can perform rapid and concurrent tear collection and glucose measurement was proposed. The tear-glucose device was composed of a strip-type electrochemical sensor modified to collect 0.4 μl of tear fluid, a 3D printed lid to safely protect eye surface from irritation or damage. The tear-glucose device could collect tear fluid within 2 seconds and simultaneously measure the tear

concentration, and thus could avoid sample transfer from tear collector to the reader. The tear-glucose device detected glucose concentration as low as 0.01 mM, and thus could sufficiently measure tear glucose concentration in vivo, which was reported to be in range of 0 ~ 0.6 mM. Using the tear-glucose device in vivo, the tear glucose concentration was observed to have high correlation to the blood glucose concentration, with 15 to 30 minutes of lag time. The response of tear glucose concentration according to the change of blood glucose was found to be different among the tested animals, and this was considered to be inherent. However, the correlation between the blood glucose and the tear glucose in an individual animal was found to be linear. Therefore, it could be envisioned that the tear glucose sensor could be applied for practical diagnosis of diabetes mellitus after obtaining the personalized correlation of the patient. Also, future researches could focus on finding a more accurate general correlation with a larger number of animals or human subjects.

In chapter 3, an implantable magnetic pump was developed to release reproducible amount of exenatide upon actuation by external magnetic field. The pump was actuated only by the patterned external magnetic field, so that it could prevent unintended actuations caused by any single magnet that can be found in our daily lives. In addition, the pump could be used semi-permanently because it does not need batteries to be powered, and the drug in the drug container can be refilled. From the animal experiment, it was found that the pharmacokinetics and the pharmacodynamics in Pump-Ex group were insignificantly different from Inj-Ex group. The magnetic pump did not induce significant immune reaction or fibrosis. Therefore, the results indicated that the magnetic pump could be used to replace needed injections.

There can be concerns about possible interaction with magnetic resonance (MR) imaging as the plunger and the barrel are made of patterned magnets. For MR compatibility, a rotatable patterned magnet can be adopted in the future, like the magnetic part embedded in MR-compatible cochlear implants. For further safety, mechanical locking system can also be included to prevent movement of plunger in MR imaging system.

The methodologies of minimally-invasive diagnosis and drug therapy proposed in this study showed comparable accuracy and efficacies to conventionally used invasive methodologies. Therefore, it could be envisioned that the methodologies suggested herein could be a patient-friendly alternative. In the future, enhanced patient acceptability would be demanded in addition to minimal invasiveness. Thus, there should be continuous effort to improve patient acceptability, such as combining the tear glucose sensor with contact lenses, which are already accepted in daily life. In the same sense, the implantable drug delivery devices could be fabricated in small sizes so that implantation would be easier, and the device would be less visible from outside.

References

1. Saeedi P, Petersohn I, Salpea P, Malanda B, Karuranga S, Unwin N, et al. Global and regional diabetes prevalence estimates for 2019 and projections for 2030 and 2045: Results from the International Diabetes Federation Diabetes Atlas, 9th edition. *Diabetes Res Clin Pr.* 2019;157.
2. IDF Diabetes Atlas, 9th ed. Brussels, Belgium: International Diabetes Federation; 2019.
3. Bartha JL, Martinez-Del-Fresno P, Comino-Delgado R. Early diagnosis of gestational diabetes mellitus and prevention of diabetes-related complications. *Eur J Obstet Gynecol Reprod Biol.* 2003;109(1):41-4.
4. Clark CM, Fradkin JE, Hiss RG, Lorenz RA, Vinicor F, Warren-Boulton E. Promoting early diagnosis and treatment of type 2 diabetes: the National Diabetes Education Program. *JAMA.* 2000;284(3):363-5.
5. Meeto DD, McAllister G, West A. Assessing glycaemic control: self-monitoring of blood glucose. *Br J Nurs.* 2011;20(15):919-20, 22, 24-5.
6. Feingold KRJE. Oral and Injectable (Non-insulin) Pharmacological Agents for Type 2 Diabetes. 2020.
7. Heinemann L. Finger pricking and pain: a never ending story. *J Diabetes Sci Technol.* 2008;2(5):919-21.
8. Richardson T, Kerr D. Skin-related complications of insulin therapy - Epidemiology and emerging management strategies. *Am J Clin Dermatol.* 2003;4(10):661-7.
9. Peyrot M, Barnett AH, Meneghini LF, Schumm-Draeger PM. Factors associated with injection omission/non-adherence in the Global Attitudes of Patients and Physicians in Insulin Therapy study. *Diabetes Obes Metab.* 2012;14(12):1081-7.
10. Aronson R. The role of comfort and discomfort in insulin therapy. *Diabetes Technol Ther.* 2012;14(8):741-7.
11. Osterberg L, Blaschke T. Adherence to medication. *N Engl J Med.* 2005;353(5):487-97.
12. Lee H, Hong YJ, Baik S, Hyeon T, Kim DH. Enzyme-Based Glucose

Sensor: From Invasive to Wearable Device. *Adv Healthc Mater.* 2018;7(8):e1701150.

13. Baca JT, Finegold DN, Asher SA. Tear glucose analysis for the noninvasive detection and monitoring of diabetes mellitus. *Ocul Surf.* 2007;5(4):280-93.

14. Yan Q, Peng B, Su G, Cohan BE, Major TC, Meyerhoff ME. Measurement of tear glucose levels with amperometric glucose biosensor/capillary tube configuration. *Anal Chem.* 2011;83(21):8341-6.

15. Baca JT, Taormina CR, Feingold E, Finegold DN, Grabowski JJ, Asher SA. Mass spectral determination of fasting tear glucose concentrations in nondiabetic volunteers. *Clin Chem.* 2007;53(7):1370-2.

16. Cameron BD, Li Y. Polarization-based diffuse reflectance imaging for noninvasive measurement of glucose. *J Diabetes Sci Technol.* 2007;1(6):873-8.

17. Stuart DA, Yonzon CR, Zhang XY, Lyandres O, Shah NC, Glucksberg MR, et al. Glucose sensing using near-infrared surface-enhanced Raman spectroscopy: Gold surfaces, 10-day stability, and improved accuracy. *Analytical Chemistry.* 2005;77(13):4013-9.

18. Mehmeti E, Stankovic DM, Chaiyo S, Zavasnik J, Zagar K, Kalcher K. Wiring of glucose oxidase with graphene nanoribbons: an electrochemical third generation glucose biosensor. *Microchim Acta.* 2017;184(4):1127-34.

19. Hwang DW, Lee S, Seo M, Chung TD. Recent advances in electrochemical non-enzymatic glucose sensors - A review. *Anal Chim Acta.* 2018;1033:1-34.

20. Peng B, Lu J, Balijepalli AS, Major TC, Cohan BE, Meyerhoff ME. Evaluation of enzyme-based tear glucose electrochemical sensors over a wide range of blood glucose concentrations. *Biosens Bioelectron.* 2013;49:204-9.

21. Liu C, Sheng Y, Sun Y, Feng J, Wang S, Zhang J, et al. A glucose oxidase-coupled DNAzyme sensor for glucose detection in tears and saliva. *Biosens Bioelectron.* 2015;70:455-61.

22. Gabriel EFM, Garcia PT, Lopes FM, Coltro WKT. Paper-Based

Colorimetric Biosensor for Tear Glucose Measurements. *Micromachines-Basel*. 2017;8(4).

23. Evans M, Schumm-Draeger PM, Vora J, King AB. A review of modern insulin analogue pharmacokinetic and pharmacodynamic profiles in type 2 diabetes: improvements and limitations. *Diabetes Obes Metab*. 2011;13(8):677-84.

24. Garber AJ. Long-acting glucagon-like peptide 1 receptor agonists: a review of their efficacy and tolerability. *Diabetes Care*. 2011;34 Suppl 2:S279-84.

25. Meier JJ. GLP-1 receptor agonists for individualized treatment of type 2 diabetes mellitus. *Nat Rev Endocrinol*. 2012;8(12):728-42.

26. Rosenstock J, Buse JB, Azeem R, Prabhakar P, Kjemis L, Huang H, et al. Efficacy and Safety of ITCA 650, a Novel Drug-Device GLP-1 Receptor Agonist, in Type 2 Diabetes Uncontrolled With Oral Antidiabetes Drugs: The FREEDOM-1 Trial. *Diabetes Care*. 2018;41(2):333-40.

27. Pons-Faudoa FP, Ballerini A, Sakamoto J, Grattoni A. Advanced implantable drug delivery technologies: transforming the clinical landscape of therapeutics for chronic diseases. *Biomed Microdevices*. 2019;21(2):47.

28. Spaan NA, Teplova AE, Renard E, Spaan JA. Implantable insulin pumps: an effective option with restricted dissemination. *Lancet Diabetes Endocrinol*. 2014;2(5):358-60.

29. Lee SH, Lee YB, Kim BH, Lee C, Cho YM, Kim SN, et al. Implantable batteryless device for on-demand and pulsatile insulin administration. *Nat Commun*. 2017;8:15032.

30. Scherz W, Doane MG, Dohlman CH. Tear volume in normal eyes and keratoconjunctivitis sicca. *Albrecht Von Graefes Arch Klin Exp Ophthalmol*. 1974;192(2):141-50.

31. Mishima S, Gasset A, Klyce SD, Jr, Baum JL. Determination of tear volume and tear flow. *Invest Ophthalmol*. 1966;5(3):264-76.

32. La Belle JT, Adams A, Lin CE, Engelschall E, Pratta B, Cook CB. Self-monitoring of tear glucose: the development of a tear based glucose sensor as an alternative to self-monitoring of blood glucose. *Chem Commun*.

2016;52(59):9197-204.

33. Haggerty CM, Larke JR. Human tear protein fractions during waking hours. *Ophthalmic Physiol Opt.* 1982;2(3):187-91.
34. Vansetten GB, Stephens R, Tervo T, Salonen EM, Tarkkanen A, Vaheri A. Effects of the Schirmer Test on the Fibrinolytic System in the Tear Fluid. *Exp Eye Res.* 1990;50(2):135-41.
35. Daum KM, Hill RM. Human tears: glucose instabilities. *Acta Ophthalmol (Copenh).* 1984;62(4):530-6.
36. Rohit A, Stapleton F, Brown SHJ, Mitchell TW, Willcox MDP. Comparison of Tear Lipid Profile among Basal, Reflex, and Flush Tear Samples. *Optometry Vision Sci.* 2014;91(12):1391-5.
37. Tan T, Watts SW, Davis RP. Drug delivery: enabling technology for drug discovery and development. *iPRECIO (R) Micro Infusion Pump: programmable, refillable, and implantable.* *Front Pharmacol.* 2011;2.
38. Cobo A, Sheybani R, Tu HD, Meng E. A wireless implantable micropump for chronic drug infusion against cancer. *Sensor Actuat a-Phys.* 2016;239:18-25.
39. Farra R, Sheppard NF, McCabe L, Neer RM, Anderson JM, Santini JT, et al. First-in-Human Testing of a Wirelessly Controlled Drug Delivery Microchip. *Sci Transl Med.* 2012;4(122).
40. Cha KH, Jensen GC, Balijepalli AS, Cohan BE, Meyerhoff ME. Evaluation of Commercial Glucometer Test Strips for Potential Measurement of Glucose in Tears. *Analytical Chemistry.* 2014;86(3):1902-8.
41. Norn MS. Conjunctival Sensitivity in Normal Eyes. *Acta Ophthalmol.* 1973;51(1):58-66.
42. Lee SH, Cho YC, Nam DY, Huh BK, Kim SN, Lee DH, et al. Designing Minimally Invasive Preocular Contact Tips for Potential Application in Tear Collection. *Cornea.* 2018;37(9):1163-8.
43. Cha KH, Qin Y, Meyerhoff ME. Origin of Low Detection Limit and High Selectivity of Roche Accu-Chek Test Strips that Enables Measurement of Tear Glucose Levels. *Electroanal.* 2015;27(3):670-6.
44. Chu MX, Miyajima K, Takahashi D, Arakawa T, Sano K, Sawada S, et

- al. Soft contact lens biosensor for in situ monitoring of tear glucose as non-invasive blood sugar assessment. *Talanta*. 2011;83(3):960-5.
45. Clarke WL, Cox D, Gonderfrederick LA, Carter W, Pohl SL. Evaluating Clinical Accuracy of Systems for Self-Monitoring of Blood-Glucose. *Diabetes Care*. 1987;10(5):622-8.
46. Clarke WL. The original Clarke Error Grid Analysis (EGA). *Diabetes Technol Ther*. 2005;7(5):776-9.
47. Korb DR, Herman JP, Finnemore VM, Exford JM, Blackie CA. An evaluation of the efficacy of fluorescein, rose bengal, lissamine green, and a new dye mixture for ocular surface staining. *Eye Contact Lens*. 2008;34(1):61-4.
48. Zhang J, Hodge W, Hutnick C, Wang X. Noninvasive diagnostic devices for diabetes through measuring tear glucose. *J Diabetes Sci Technol*. 2011;5(1):166-72.
49. Vashist SK. Non-invasive glucose monitoring technology in diabetes management: a review. *Anal Chim Acta*. 2012;750:16-27.
50. Taormina CR, Baca JT, Asher SA, Grabowski JJ, Finegold DN. Analysis of tear glucose concentration with electrospray ionization mass spectrometry. *J Am Soc Mass Spectrom*. 2007;18(2):332-6.
51. Collins RE, Cooke CE. Fundamental Basis for the Contact Angle and Capillary Pressure. *T Faraday Soc*. 1959;55(9):1602-6.
52. Patane MA, Schubert W, Sanford T, Gee R, Burgos M, Isom WP, et al. Evaluation of Ocular and General Safety Following Repeated Dosing of Dexamethasone Phosphate Delivered by Transscleral Iontophoresis in Rabbits. *J Ocul Pharmacol Th*. 2013;29(8):760-9.
53. Al-Achi A, Gupta MR, Stagner WC. *Integrated pharmaceuticals: applied preformulation, product design, and regulatory science*: John Wiley & Sons; 2013.
54. Lane JD, Krumholz DM, Sack RA, Morris C. Tear glucose dynamics in diabetes mellitus. *Curr Eye Res*. 2006;31(11):895-901.
55. Unwin N, Shaw J, Zimmet P, Alberti KGMM. Impaired glucose tolerance and impaired fasting glycaemia: the current status on definition

- and intervention. *Diabetic Med.* 2002;19(9):708-23.
56. Portha B, Giroix MH, Tourrel-Cuzin C, Le-Stunff H, Movassat J. The GK rat: a prototype for the study of non-overweight type 2 diabetes. *Methods Mol Biol.* 2012;933:125-59.
57. Simonsen L, Pilgaard S, Orskov C, Hartmann B, Holst JJ, Deacon CF. Long-term exendin-4 treatment delays natural deterioration of glycaemic control in diabetic Goto-Kakizaki rats. *Diabetes Obes Metab.* 2009;11(9):884-90.
58. Balkan B, Kwasnik L, Miserendino R, Holst JJ, Li X. Inhibition of dipeptidyl peptidase IV with NVP-DPP728 increases plasma GLP-1 (7-36 amide) concentrations and improves oral glucose tolerance in obese Zucker rats. *Diabetologia.* 1999;42(11):1324-31.
59. Gedulin BR, Nikoulina SE, Smith PA, Gedulin G, Nielsen LL, Baron AD, et al. Exenatide (Exendin-4) improves insulin sensitivity and beta-cell mass in insulin-resistant obese fa/fa Zucker rats independent of glycemia and body weight. *Endocrinology.* 2005;146(4):2069-76.
60. Linder M, Huther S, Reinacher M. In vivo reactions in mice and in vitro reactions in feline cells to implantable microchip transponders with different surface materials. *Vet Rec.* 2009;165(2):45-50.
61. Zheng XM, Li Y, Fu G, Gong M. Application of novel peptide (Pp1) improving the half-life of exendin-4 in vivo. *Peptides.* 2011;32(5):964-70.
62. Gibney MA, Arce CH, Byron KJ, Hirsch LJ. Skin and subcutaneous adipose layer thickness in adults with diabetes at sites used for insulin injections: implications for needle length recommendations. *Curr Med Res Opin.* 2010;26(6):1519-30.
63. Szayna M, Doyle ME, Betkey JA, Holloway HW, Spencer RGS, Greig NH, et al. Exendin-4 decelerates food intake, weight gain, and fat deposition in Zucker rats. *Endocrinology.* 2000;141(6):1936-41.
64. Greig NH, Holloway HW, De Ore KA, Jani D, Wang Y, Zhou J, et al. Once daily injection of exendin-4 to diabetic mice achieves long-term beneficial effects on blood glucose concentrations. *Diabetologia.* 1999;42(1):45-50.

65. Matsuda M, DeFronzo RA. Insulin sensitivity indices obtained from oral glucose tolerance testing - Comparison with the euglycemic insulin clamp. *Diabetes Care*. 1999;22(9):1462-70.
66. Koyama M, Wada R, Sakuraba H, Mizukami H, Yagihashi S. Accelerated loss of islet beta cells in sucrose-fed Goto-Kakizaki rats, a genetic model of non-insulin-dependent diabetes mellitus. *Am J Pathol*. 1998;153(2):537-45.
67. Kenneth Ward W. A review of the foreign-body response to subcutaneously-implanted devices: the role of macrophages and cytokines in biofouling and fibrosis. *J Diabetes Sci Technol*. 2008;2(5):768-77.
68. Yu M, Benjamin MM, Srinivasan S, Morin EE, Shishatskaya EI, Schwendeman SP, et al. Battle of GLP-1 delivery technologies. *Adv Drug Deliv Rev*. 2018;130:113-30.
69. Young AA, Gedulin BR, Bhavsar S, Bodkin N, Jodka C, Hansen B, et al. Glucose-lowering and insulin-sensitizing actions of exendin-4: studies in obese diabetic (ob/ob, db/db) mice, diabetic fatty Zucker rats, and diabetic rhesus monkeys (*Macaca mulatta*). *Diabetes*. 1999;48(5):1026-34.
70. Joung YH. Development of implantable medical devices: from an engineering perspective. *Int Neurourol J*. 2013;17(3):98-106.
71. Campbell JE, Drucker DJ. Pharmacology, physiology, and mechanisms of incretin hormone action. *Cell Metab*. 2013;17(6):819-37.
72. Krishnan L, Dhatariya K, Gerontitis D. No clinical harm from a massive exenatide overdose - a short report. *Clin Toxicol*. 2013;51(1):61.
73. Cohen V, Teperikidis E, Jellinek SP, Rose J. Acute exenatide (Byetta) poisoning was not associated with significant hypoglycemia. *Clin Toxicol (Phila)*. 2008;46(4):346-7.
74. McCormack PL. Exenatide Twice Daily: A Review of Its Use in the Management of Patients with Type 2 Diabetes Mellitus. *Drugs*. 2014;74(3):325-51.
75. Bhatia G, Lau ME, Koury KM, Gulur P. Intrathecal Drug Delivery (ITDD) systems for cancer pain. *F1000Res*. 2013;2:96.
76. Lee SH, Ahn JW, Cho YC, Kim SN, Lee C, Ku GW, et al. Wirelessly

Controlled Implantable System for On-demand and Pulsatile Insulin Administration. *Sci Rep.* 2019;9(1):5009.

77. Marathe CS, Rayner CK, Jones KL, Horowitz M. Relationships Between Gastric Emptying, Postprandial Glycemia, and Incretin Hormones. *Diabetes Care.* 2013;36(5):1396-405.

78. Rowlands J, Heng J, Newsholme P, Carlessi R. Pleiotropic Effects of GLP-1 and Analogs on Cell Signaling, Metabolism, and Function. *Front Endocrinol.* 2018;9.

Abstract in Korean

국문 초록

많은 당뇨병 환자들이 현재 채혈을 통한 진단 방법과 주사를 통한 약물 치료를 통해 혈당을 관리하고 있다. 이런 침습적인 진단 및 투약 방식은 환자들에게 많은 고통과 트라우마, 굳은 살, 가려움증 및 염증 등의 부작용을 초래하는 문제점이 있다. 이를 해결하기 위해 본 논문에서는 당뇨병 진단 및 약물치료를 위한 최소침습 방법론을 제안하고자 한다.

먼저, 채혈 진단 방식의 대안으로 눈물 내 당 농도, 즉 누당을 측정하는 센서를 개발하였다. 누당은 혈당과 높은 상관관계를 보이는 까닭에 많은 진단 연구가 진행되었다. 그러나 많은 양의 눈물 샘플을 필요로 하며, 이를 채취하는 시간이 길어져 환자에게 불편함과 고통을 야기하는 문제점이 있었다. 또한 눈물 샘플을 채취 장치에서 측정 장치로 옮기는 과정에서 발생하는 정확도의 하락과 불편함이 문제가 되었다. 이런 문제를 해결하기 위해, 높은 정확도를 가지는 전기화학 센서를 개조하여 필요 눈물 양을 0.4 μl 로 줄였으며, 3D 프린트 된 lid 의 장착을 통하여 전안부 접촉 시에도 손상을 야기하지 않도록 하였다. 개조된 센서와 lid 의 결합으로 구성된 tear-glucose device 는 전안부에 접촉한 지 2 초 이내에 필요한 양의 샘플을 채취할 수 있었으며, 채취와 동시에 누당 농도를 측정하였다. 동물 모델에 적용한 결과, tear-glucose

device 를 통해 혈당과 누당 간의 높은 상관관계를 확인할 수 있었다. 또한, Clarke error grid analysis 결과, 개발된 tear-glucose device 를 통해 계산된 혈당값이 이미 상용화된 혈당 측정기 대비 준수한 정확도를 보였음을 확인할 수 있었다.

다음으로, 주사 약물 치료의 대안으로 이식형 약물전달 디바이스를 개발하였다. 현재 개발된 당뇨병 관리용 이식형 약물전달 디바이스의 경우, 약물치료 regimen 을 최적화하지 못하여 tachyphylaxis 를 야기하거나, 디바이스의 크기, 수명, 안전성에 문제가 있는 경우가 있었다. 이러한 문제를 해결하기 위해, 패턴화된 자기력 구동 이식형 약물전달 펌프를 개발하였다. 본 펌프는 on-demand bolus 전달 방식을 통해 최적화된 약물치료 regimen 을 구현하고, 배터리 대신 자기력 구동 방식을 사용해 디바이스의 크기, 수명 문제를 해결하고, 패턴화된 자기력을 사용함으로써 안전성 문제를 해결하였다. 또한 폴리우레탄 약물저장소를 사용하여 고체 약물저장소에서 나타나는 음압으로 인한 방출 문제를 해결하였다. 본 펌프를 평가한 결과, $11.4 \pm 0.3 \mu\text{g}$ 의 exenatide 를 약물 충전 없이 300 회 방출시킬 수 있었다. 동물 모델에서 평가한 결과, 약력학 및 약동학에서 기존 주사 약물치료와 유사한 효과를 보였다.

본 연구를 통해 개발된 누당 측정 센서와, 자기력 구동 이식형 약물전달 펌프는 기존 사용되는 혈당측정기와 주사 약물치료 방법론과 유사한 효용성을 보이는 것을 확인하였다. 따라서 이는

침습적인 당뇨병의 진단 및 약물치료 방식의 대안으로 제시될 수 있을 것이라 기대한다.

핵심어: 최소침습, 당뇨병, 혈당 측정, 누당 측정, 스트립형 누당 센서, 주사 약물치료, 자기력 구동, 이식형 약물전달 디바이스

Student number: 2017-33892

감사의 글

제 학위를 받기까지 지나온 날들을 되돌아보며 저에게 많은 도움과 영감을 주신 많은 분들께 감사의 말씀을 올리고자 합니다.

가장 먼저 저를 긴 시간 동안 지도해주신 최영빈 교수님께 감사드립니다. 교수님 덕분에 좋은 환경에서 뛰어난 동료들과 우수한 연구들을 많이 진행할 수 있었습니다. 또한 교수님께 비하면 아직 갈 길이 멀지만, 교수님 아래에서 생각하는 법을 많이 배울 수 있었습니다. 바쁘신 와중에도 함께 연구를 진행하시며 아끼지 않고 많은 지도를 해주신 조영민 교수님, 이동윤 교수님, 조양현 교수님께 감사드립니다. 또한 제 논문 심사를 맡아주신 김성완 교수님, 이정찬 교수님을 포함한 모든 바이오엔지니어링 협동 과정 교수님들께도 감사드립니다. 또한 함께 연구를 진행해 주신 민세희 선생님, 김미나 선생님, 박시진 선생님, 이철 교수님께 감사드립니다. 실험을 하는데 있어 많은 도움을 주신 이주희 선생님, 이재용 선생님, 의공학과 김화룡 선생님, 동물 실험실 이학영 선생님께도 감사의 말씀을 전합니다.

다음으로 우리 연구실 동료들, 그 중에서도 오랜 시간 동안 저를 많이 밀어준 승호 형, 형하고 이야기 한대로 내 커리어가 흘러가지는 않았지만 앞으로의 삶에도 좋은 밑바탕이 될 즐거운 시간들 있었어! 나중에 기회가 된다면 언젠가는 또 같이 일 하고 싶어요. 또 나하고 승호형에게 정말 많이 맞춰주며 긴 시간 고생한

초림이, 미안하고 고마운 점이 많고, 앞으로는 하는 연구마다 대박 나길 기원할게! 참 불가능을 가능케 만든다는 게 무엇인지 같이 경험해준 한비, 그 동안 연구하라 대화하라 많이 고생했는데, 결실을 잘 마무리해보자. 들어온 지 얼마 안되어서부터 나와 함께 머리 싸매가며 실험해준 재훈이도 누나들 잘 챙기며 고생해줘. 앞으로 랩장으로 연구실을 지켜줄 창희도 지금까지처럼 앞으로 묵묵히 할 일 잘 할 것이야. 민지 역시 오빠 언니들 잘 도와주고 잘 배웠다가 나중에 후배가 오는 날이 온다면 좋은 선배가 되길 빌게. 재영이는 곧 떠나겠지만, 열심히도 좋은데, 결과적으로 진짜 잘해야 한다. 쉽지 않아. 그리고 후배들에게 귀감이 되고 계시는 많은 선배들, 천권 형, 민이 형, 명훈이 형, 지은 누나, 성윤 누나, 수빈 누나, 병휘 형, 범강이 형, 세나 누나, 형 누나들의 조언과 에너지가 연구 생활에 많은 도움이 되었어요. 그리고 졸업하여 각자의 자리에서 실력을 발휘하고 있는 친구들과 후배들, 원석이, 영빈이, 재연이, 송아, 동연이, 지민이, 내영이, 그리고 정말 즐거운 연구 생활을 하게 해준 범수와 우미까지, 정말 많이 도와줘서 고마웠고 덕분에 좋은 연구하는데도 많은 영감을 받았어. 마지막으로 윤영이, 종인이, 동훈이, 윤서, 인화, 민구 같은 인턴 친구들 덕에 연구 생활이 더욱 수월할 수 있었어, 고마워 친구들!

함께 연구를 진행하지는 않았지만 많은 시간을 함께 지내며 서로 용기를 북돋아준 협동 과정 내 많은 동료들, 특히 믿고 의지하거나 많은 조언들을 구할 수 있었던 왕진이 형, 이사람 박사님, 지흠 누나, 정은 누나, 윤하 형, 동아 누나, 그리고 동기 같은 든든함을

준 희안이, 회원이, 치원이, 고명준이, 지훈이, 준녕이, 경모, 유쾌한 에너지를 지닌 병준이, 김명준이, 현빈이, 치현이, 순빈이, 준호, 성동석이, 우상이, 병탁이. 실험 외적으로도 많은 에너지를 준 IGM 농구팀 멤버들, 긴 시간 동안 함께 해주었던 paleshade 밴드 멤버들, SHSID, JFK, UW 친구들 모두 힘이 되주어서 고마웠어요. 앞으로도 좋은 인연 이어가며 서로서로 도와줄 수 있으면 좋겠습니다. 감사합니다.

마지막으로 제 인생에 걸쳐 정말 많은 사랑을 쏟아 주신 아버지, 어머니께 저라는 사람을 만들어 주시고, 돌봐 주시고, 기도해 주셔서 감사드립니다. 또한 군대부터 학위기간까지 어떻게 보면 인생에 가장 힘든 시기일 지 모르는 기간들을 함께 버텨주느라 마음고생 심했을 수정이, 이루 말할 수 없을 정도로 고맙고, 앞으로는 꽃 길만 걸도록 합시다! 또한 학위 기간 동안 묵묵히 응원해주시고 보살펴주신 장인어른 장모님께 정말로 큰 감사 말씀을 드립니다. 주신 사랑에 보답하여 효도하며 잘 살도록 하겠습니다. 그리고 규아는 건강하고 밝게 커주길 바랍니다. 모두들 많이 사랑합니다.

2020년 12월 27일

조 용 찬